NASA/CR—2003-212123

Jet Noise Physics and Modeling Using First-Principles Simulations

Jonathan B. Freund
University of Illinois, Urbana-Champaign, Urbana, Illinois

February 2003

The NASA STI Program Office . . . in Profile

Since its founding, NASA has been dedicated to the advancement of aeronautics and space science. The NASA Scientific and Technical Information (STI) Program Office plays a key part in helping NASA maintain this important role.

The NASA STI Program Office is operated by Langley Research Center, the Lead Center for NASA's scientific and technical information. The NASA STI Program Office provides access to the NASA STI Database, the largest collection of aeronautical and space science STI in the world. The Program Office is also NASA's institutional mechanism for disseminating the results of its research and development activities. These results are published by NASA in the NASA STI Report Series, which includes the following report types:

- TECHNICAL PUBLICATION. Reports of completed research or a major significant phase of research that present the results of NASA programs and include extensive data or theoretical analysis. Includes compilations of significant scientific and technical data and information deemed to be of continuing reference value. NASA's counterpart of peer-reviewed formal professional papers but has less stringent limitations on manuscript length and extent of graphic presentations.

- TECHNICAL MEMORANDUM. Scientific and technical findings that are preliminary or of specialized interest, e.g., quick release reports, working papers, and bibliographies that contain minimal annotation. Does not contain extensive analysis.

- CONTRACTOR REPORT. Scientific and technical findings by NASA-sponsored contractors and grantees.

- CONFERENCE PUBLICATION. Collected papers from scientific and technical conferences, symposia, seminars, or other meetings sponsored or cosponsored by NASA.

- SPECIAL PUBLICATION. Scientific, technical, or historical information from NASA programs, projects, and missions, often concerned with subjects having substantial public interest.

- TECHNICAL TRANSLATION. English-language translations of foreign scientific and technical material pertinent to NASA's mission.

Specialized services that complement the STI Program Office's diverse offerings include creating custom thesauri, building customized databases, organizing and publishing research results . . . even providing videos.

For more information about the NASA STI Program Office, see the following:

- Access the NASA STI Program Home Page at ***http://www.sti.nasa.gov***

- E-mail your question via the Internet to help@sti.nasa.gov

- Fax your question to the NASA Access Help Desk at 301–621–0134

- Telephone the NASA Access Help Desk at 301–621–0390

- Write to:
  NASA Access Help Desk
  NASA Center for AeroSpace Information
  7121 Standard Drive
  Hanover, MD 21076

NASA/CR—2003-212123

Jet Noise Physics and Modeling Using First-Principles Simulations

Jonathan B. Freund
University of Illinois, Urbana-Champaign, Urbana, Illinois

Prepared under Grant NAG3–2662

National Aeronautics and
Space Administration

Glenn Research Center

February 2003

Acknowledgments

Support for this work, provided by NASA, is very gratefully acknowledged.

This report contains preliminary findings, subject to revision as analysis proceeds.

The Propulsion and Power Program at NASA Glenn Research Center sponsored this work.

Available from

NASA Center for Aerospace Information
7121 Standard Drive
Hanover, MD 21076

National Technical Information Service
5285 Port Royal Road
Springfield, VA 22100

Available electronically at http://gltrs.grc.nasa.gov

Jet Noise Physics and Modeling Using First-Principles Simulations

Jonathan B. Freund
University of Illinois, Urbana-Champaign
Urbana, Illinois 62801

Accomplishments of this year are in four categories, which are summarized here. Detailed appendices are attached as appropriate.

1 Noise and source statistics relevant to the MGBK framework

An extensive analysis of our jet DNS database has provided for the first time the complex correlations that are the core of many statistical jet noise models, including MGBK. We have also for the first time explicitly computed the noise from different components of a commonly used noise source as proposed in many modeling approaches. Key findings are:

1. While two-point (space and time) velocity statistics are well-fitted by decaying exponentials, even for our low-Reynolds-number jet, spatially integrated fourth-order space/retarded-time correlations which constitute the noise "source" in MGBK and are instead well-fitted by Gaussians. The width of these Gaussians depends (by a factor of 2) on which components are considered. This is counter to current modeling practice.

2. A standard decomposition of the Lighthill source is shown by direct evaluation to be somewhat artificial since the noise from these nominally separate components is in fact highly correlated. We anticipate that the same will be the case for the Lilley source.

3. The far-field sound is computed in a way that explicitly includes all quadrupole cancellations, yet evaluating the Lighthill integral for only small part of the jet yields a far-field noise far louder than that from the whole jet due to missing non-quadrupole cancellations.

Details of this study are discussed in a draft of a paper included as appendix A.

2 Large-scale dynamics and large-eddy simulation

It seems that the noise from a jet is primarily due to the locally largest and most energetic scales, making large-eddy simulation (LES) potentially effective for predicting jet noise. At the same time the dynamics of the very large scales in a jet are of high interest from the perspective of understanding the mechanics of noise generation. Our work in this area follows several related paths, some in collaboration with Prof. Lele's group at Stanford.

2.1 Large-scale structural dynamics – quantitative

We have designed spatial filters that remove small-scale, acoustically irrelevant components of the jet's turbulence. These filtered fields are being used in two ways. In the first, we use the DNS to provide an "ideal" (determined *a priori*) sub-grid-scale model that is used to close linearized equations for these large-scales,

$$\frac{\partial}{\partial t}\rho^{(L)} + \frac{\partial}{\partial x_j}\left(\overline{\rho}u_j^{(L)} + \rho^{(L)}\overline{u}_j\right) = \frac{\partial}{\partial x_j}\left(\widetilde{\rho u}_j - \widetilde{\rho u_j}\right)$$

$$\frac{\partial}{\partial t}\left(\overline{\rho}u_i^{(L)} + \rho^{(L)}\overline{u}_i\right) + \frac{\partial}{\partial x_j}\left(\overline{\rho u}_i u_j^{(L)} + \overline{\rho}u_i^{(L)}\overline{u}_j + \rho^{(L)}\overline{u}_i\overline{u}_j + p^{(L)}\delta_{ij}\right) = \frac{\partial}{\partial t}\left(\widetilde{\rho u}_j - \widetilde{\rho u_j}\right) + \frac{\partial}{\partial x_j}\left(\widetilde{\rho u}_i\widetilde{u}_j - \widetilde{\rho u_i u_j}\right)$$

$$\frac{\partial}{\partial t}\left(\overline{\rho}E^{(L)} + \rho^{(L)}\overline{E}\right) + \frac{\partial}{\partial x_j}\left(\left[\overline{\rho}\overline{E} + \overline{p}\right]u_j^{(L)} + \left[\rho^{(L)}\overline{E} + \overline{\rho}E^{(L)} + p^{(L)}\right]\overline{u}_j\right) = \frac{\partial}{\partial t}\left(\widetilde{\rho}\widetilde{E} - \widetilde{\rho E}\right) + \frac{\partial}{\partial x_j}\left(\left[\widetilde{\rho}\widetilde{E} + \widetilde{p}\right]\widetilde{u}_j - \left(\widetilde{\rho E u_j} + \widetilde{p u_j}\right)\right).$$

This will allow us to explicitly study their dynamics. Figure 1 shows the effect of filters of various widths on the turbulence. Despite the dramatic effect of the filter on the appearance of the turbulence, flow quantities remain essentially unaltered in the region of frequency/streamwise-wavenumber (k–ω) space that is capable of radiating to the far field (figure 2). The evolution equations are currently being solved to identify the effect of the sub-grid-scales on the evolution of the structures capable of radiating to the far field and the dynamics of these structure as they interact with the mean flow. This part of the work is in close collaboration with Sanjiva Lele and his student Dan Bodony.

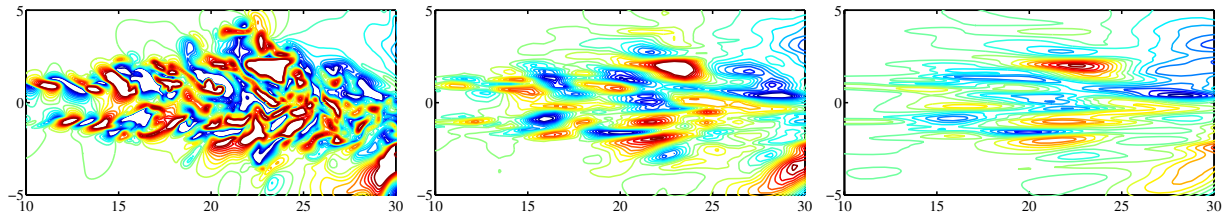

Figure 1: The v_θ field. Left: unfiltered; middle: filtered with $\ell = 2.5r_o$; and right: filtered with $\ell = 5.0r_o$. These filters define our very large scales.

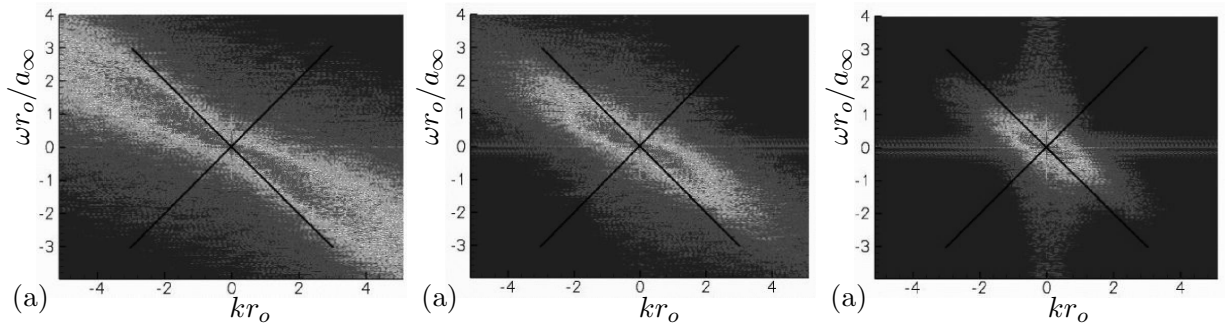

Figure 2: Frequency/streamwise-wavenumber makeup of the data: (a) unfiltered, (b) filtered with $\ell = 2.5r_o$, (c) filtered with $\ell = 5.0r_o$. The straight lines separate regions that can not radiate to the far field in r (subsonic phase velocity in the right and left wedges) from those can can radiate to the far field in r (supersonic phase velocity in the top and bottom wedges).

2.2 Large-scale structural dynamics – qualitative

In the past, we have not been able to identify noisy events based on visualizations. However, with much of the non-radiating turbulence removed by the selective filtering procedure described above we are revisiting this approach. Many quantities (in fact all that we can think of) are being investigated. Sample movies showing simultaneously the far- and near-field pressure for the full field and a highly streamwise and azimuthally filtered near field are at

`http://taylor.tam.uiuc.edu/~jfreund/migall.gif` and at

`http://taylor.tam.uiuc.edu/~jfreund/mig5.0.gif`,

respectively. We have also started making visualizations that take into account the retarded time. In this case flow quantities $q(\mathbf{x}, t)$ are plotted at $q(\mathbf{x}, \tau) = q(\mathbf{x}, t - |\mathbf{x}_l - \mathbf{x}|/a_\infty)$ for listener points $\mathbf{x}_l$. We anticipate that this view will be more relevant for the far-field sound.

2.3 Direct evaluation of mode conversion

With the data in k–ω coordinates it is possible to explicitly compute the convolutions (products in real coordinates) that put energy into modes that radiate. The entire machinery has been assembled to do this and some initial convolutions was computed, but a subtle "bug" was found and the procedure is being rerun. While this approach can precisely identify what types of interactions convert turbulent energy to radiation components, it has the drawback that the spectral-space data no longer have an immediate interpretation in physical coordinates. Thus, this method will be used in close conjunction with the more "dynamical" approach above. Just as figures 1 and 2 are complementary, once the dynamic simulation for the very large scale modes are solved, similar interpretations in k–ω space will deepen understanding.

2.4 Large-eddy simulation (LES)

We collaborated with Benjamin Rembold at the Center for Turbulence Research this summer to compute the sound from a large-eddy simulation of a turbulent jet. In particular, we were looking for errors due explicitly to the sub-grid-scale models in the LES. Figure 3 (a) shows that the $\alpha = 30^\circ$ spectrum of this jet is well predicted and in good agreement with the corresponding DNS spectrum shown in figure 3 (b) and in general agreement with other jet data at similar Reynolds numbers. However, at upstream angles the spectra in 3 (c) and (d) show that the LES has created substantial spurious noise. We are investigating the reasons for this. We see two possible causes. One is explicit numerical errors due to "pushing" the resolution limit as is common practice in LES. The other is

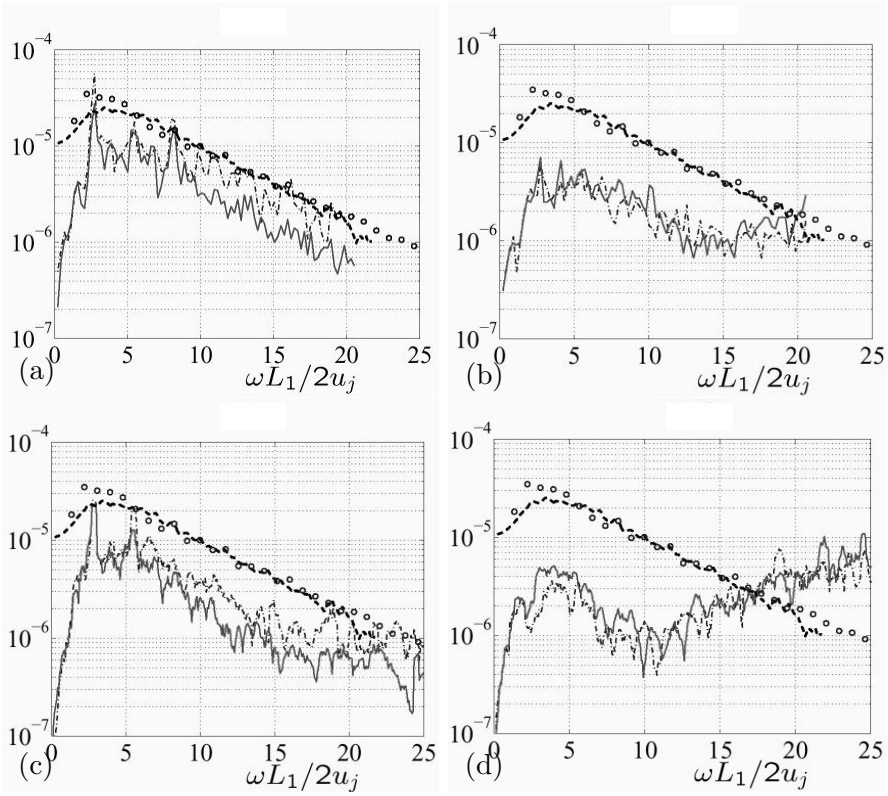

Figure 3: Far-field noise spectra: (a) DNS at $\alpha = 30°$; (b) DNS at $\alpha = 150°$; (c) LES at $\alpha = 30°$; and (d) LES at $\alpha = 150°$. This is for a 5:1 rectangular jet with —— the major plane and —— the minor plane. For reference, we also show - - - - the low-Reynolds-number round jet of Stromberg[1] (experiment) and ∘ the low-Reynolds-round jet of Freund[2] (DNS).

direct radiation by the sub-grid-scale model, which are universally designed to model turbulence dynamics not noise.

3 Flow acoustic interactions

This past year we published a journal article (Appendix B) which showed qualitatively, based on ray trajectories traced through unsteady jet turbulence, that jet turbulence can substantially scatter noise. In collaboration with Tom Bewley and Laura Cerveno at UCSD we have extended the adjoint based control procedure we use at UIUC to control jet noise to numerically compute an adjoint Green's function for the unsteady jet flow. This provides both the quantitative amplitudes that were missing in the ray tracing study, and at the same time provides the effective forward Green's function for a single far-field direction with one computation, the same way Tam's[3] approach does for a steady jet flow. Figure 4 shows preliminary computations of the adjoint Green's function

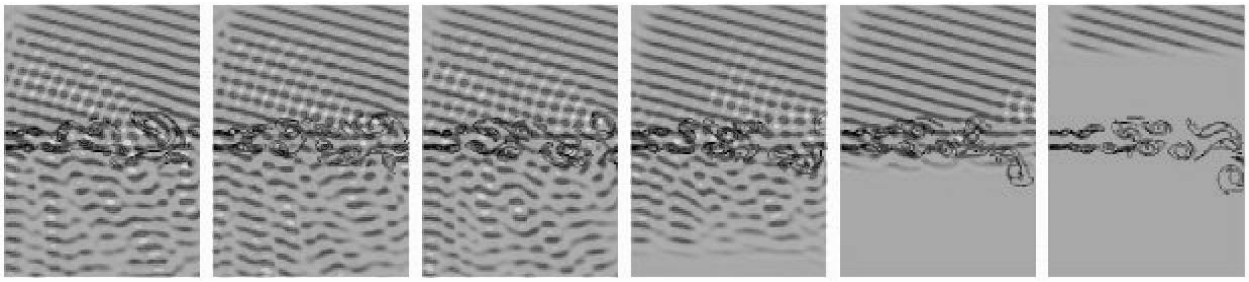

Figure 4: Adjoint Green's function for an unsteady two-dimensional jet flow at several instances. The vorticity is shown by the black contours.

for a two-dimensional jet. We see the substantial effect of the unsteady unsteady two-dimensional turbulence structures.

4 Near-nozzle mixing layer DNS

We have designed a new algorithm to compute both a hot and cold near nozzle jet mixing layer. (A previous simulation was found to be effectively forced by the inflow disturbance rendering it less useful for studying certain statistical representations of noise sources.) We have a mapped spectral code and a de-aliased mapped spectral code that are being developed by John Moreland, a graduate student of the PI. He is working out inflow conditions and zonal boundary conditions to do the large simulations. Figure 5 shows visualization of the mixing layer computed with the de-aliased code. There is clearly significant work to do to with regard to the inflow conditions, which have proved more difficult than anticipated. Any excitation that we impose will necessarily force the flow. In the past we "fed" turbulence from a streamwise periodic simulation into the domain for a jet simulation,[4] but there remained a small artifact of the particular excitation far downstream.[5] Our Mach 0.9 jet, which has a laminar inflow region excited by very random, very low amplitude perturbations seems to be our best approach so far. Unfortunately, we do not know what the disturbances are in reality because precise nozzle exit conditions are seldom reported.

A Turbulent Jet Noise: Shear Noise, Self-Noise and Other Contributions

Abstract

Using a previously validated simulation database of a Mach 0.9 cold jet, we examine the components of Lighthill's analogous noise source that are linear (shear noise terms) and quadratic

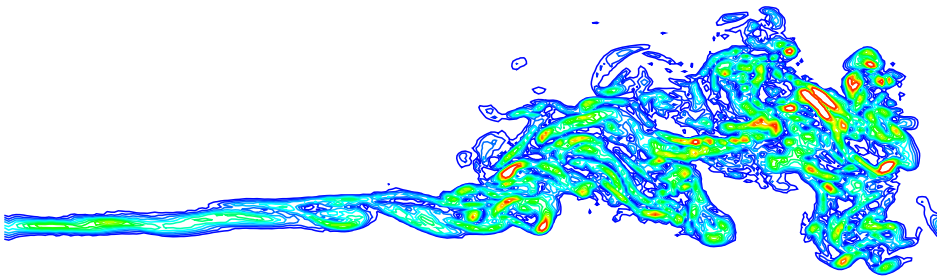

Figure 5: Preliminary results of de-aliased mapped spectral method code shoing vorticity of a $M = 0.9$ mixing layer.

(self-noise terms) in velocity fluctuations, as well as components that are deviations from $p' = a_\infty^2 \rho'$. It is found that the shear noise is highly directional, with an angle of extinction near $\alpha = 90°$, measured from the downstream axis, which is consistent with Ribner's theory[6] that $I \sim \cos^4 \alpha + \cos^2 \alpha$. Its spectrum broadens at larger α. In contrast, the self-noise is more uniform. Is is fit by five inverse Doppler factors, $(1 - M_c \cos \alpha)^{-5}$, but only provided that M_c is dropped below its typically assumed values of $M_c \approx 0.6 U_j / a_\infty = 0.5$ to $M_c \approx 0.3$. In previous work it was found that $M_c \approx 0.3$ was indeed the dominant phase velocity for the Lighthill source in this same jet. The spectral shape of the self-noise is relatively independent of angle, in contrast to the shear noise. The shear noise and self-noise are correlated, especially at small angles where their mutual correlation coefficient reaches as low as -0.4, casting doubt on models that treat these terms as distinct. The $p' = a_\infty^2 \rho'$ contribution is relatively small, not negligible as expected for a cold jet, but it is so well correlated with the shear noise (correlation coefficient of -0.6 at small angles) that it should not be neglected. The total radiated power of the component quadratic in the velocity fluctuations is nearly the same as that of all components combined. Examining turbulence statistics relevant to jet noise, we see that two-point correlations statics are well fitted by exponential functions, as is typical of turbulence at all but the lowest Reynolds numbers, but integrated fourth-order space/retarded-time covariances, which are directed related to the radiated acoustic intensity, are instead very well fitted by Gaussian functions of different widths for different components, which is counter to conventional modeling practice.

A.1 Background and objectives

Several attempts to model jet noise[6–11] have followed the standard Reynolds decomposition of the flow variables: $q = \bar{q} + q'$, where q is a flow quantity and $\bar{q}$ and q' are its average and an instantaneous perturbation. This study uses a numerical simulation database to examine this decomposition as it is typically used in jet noise models utilizing Lighthill's theory.

Lighthill's equation[12] can be written

$$\frac{\partial^2 \rho'}{\partial t^2} - a_\infty^2 \frac{\partial^2 \rho'}{\partial x_j \partial x_j} = \frac{\partial^2 T_{ij}}{\partial x_i \partial x_j}, \tag{1}$$

where $T_{ij} = \rho u_i u_j + (p - a_\infty^2 \rho)\delta_{ij} - \tau_{ij}$ is the Lighthill stress tensor, a_∞ is the ambient sound speed, τ_{ij} is the viscous stress, and ρ' is a density fluctuation. The double divergence of T_{ij} appearing on the right hand side of (1) serves as a nominal acoustic source, but its use here should not be interpreted in any way as an attempt to define the true noise source in the jet, if there is such a thing. Such an interpretation is impractical for at least two reasons. The first, which has been well understood starting with Lighthill's original derivation of (1), is that all effects aside from propagation in a homogeneous stationary medium, such as refraction, are lumped into this nominal source. More sophisticated theories attempt to treat mean-flow refraction explicitly,[13–15] but are more analytically challenging. The second is that most of $T_{ij,ij}$ does not radiate to the far acoustic field, which is also widely understood. What $T_{ij,ij}$ does provide us is an exact connection between near-field turbulence statistics and their noise. This is how we use it.

Applying the Reynolds decomposition to T_{ij} gives

$$T_{ij} = \bar{T}_{ij} + \underbrace{\rho(\bar{u}_i u_j' + u_i' \bar{u}_j)}_{\text{shear}} + \underbrace{\rho u_i' u_j'}_{\text{self}} + \underbrace{(p' - a_\infty^2 \rho')\delta_{ij}}_{\text{entropy}} - \underbrace{\tau_{ij}'}_{\text{viscous}}, \tag{2}$$

where source terms that are linear in the fluctuating velocities have been labeled 'shear' to reflect that this source component entails turbulent fluctuations interacting with the sheared mean flow, and source terms that are quadratic in the fluctuating velocities have been labeled 'self' to reflect that this source component entails turbulent fluctuation interacting with themselves. For clarity we have not yet decomposed ρ into $\bar{\rho}$ and ρ'. The so-called entropic contribution has often been neglected to facilitate analysis,[12,16] but is thought by some to be significant for both hot and cold jets, having an efficient dipole component.[15,17] Lighthill[12] stated emphatically

that the viscous component of T_{ij} could be neglected with respect to the far-field sound, and this view has held.[15,16] An implicit result of Colonius & Freund's[18] computation of jet noise using Lighthill's analogy was that τ_{ij} does not contribute substantially even at $Re = 2000$.

Until now, there has been no direct measurements to verify the modeling of different components, only of the net result. A common modeling assumption is that the self-noise and shear noise contributions are independent, the validity of which is untested. We use an existing well-validated the direct numerical simulation database to directly evaluate the role of the different components. Turbulence statistics that constitute noise sources, but are also difficult to measure experimentally, are also computed to evaluate common modeling practice and identify scalings.

A.2 Simulation Database

The database we use was reported on in detail by Freund.[2] It is a Mach 0.9, Reynolds number 3600, constant stagnation temperature ($T_j/T_\infty = 0.86$) jet. It has been validated against the corresponding experimental results of Stromberg,[1] matching the mean flow development, sound pressure level directivity at $60r_o$ (60 jet radii) from the nozzle, and sound spectrum at $\alpha = 30°$. Because of its low Reynolds number, this jet has laminar shear layers that transition before the end of the potential core. After transition, its turbulence has broad-banded energy spectra, rapidly decaying two-point correlations, and viscous dissipation is a significant component in the turbulent kinetic energy budget. Reynolds stresses downstream of the potential core match those measured in higher-Reynolds-number experiments.

Despite this agreement with some aspects of high-Reynolds-number turbulence, we must remain aware in interpreting our results that there are qualitative differences in the noise from a low- versus high-Reynolds-number jet. Most notably, the spectrum of a high-Reynolds-number jet is broader because of the greater range of turbulence scales in the flow. There are two general factors that might cause this. The first is that broadening of local turbulence spectra leads to higher frequency noise. However, these fine scales contain relatively little energy, making it more likely that the high frequencies missing at low Reynolds numbers instead come from energetic structures in the shear layers near the nozzle. These near-nozzle shear layer structures are higher frequency by virtue of their smaller size. Statistical arguments support this. Lighthill's[19] arguments suggest that most of the noise comes from "eddies only slightly smaller than the main energy bearing eddies." Similarly, noise source localization experiments[20] have show that most of the high-frequency noise has an apparent origin in the thin shear layers near the nozzle. Under this interpretation, a low-Reynolds-number jet can be viewed as a model for that portion of a high-Reynolds-number jet near and beyond the close of the potential core. Some additional Reynolds number sensitive turbulence correlations relevant to noise are discussed later in this paper.

The flow simulation used $N_x \times N_r \times N_\theta = 640 \times 250 \times 160$ points in the axial, radial and azimuthal directions, respectively. Data were stored on every other mesh point in all three coordinate directions every 20 numerical time steps of $\Delta t = 0.0085 r_o/a_\infty$ each, which corresponds to a Strouhal number $St = 14.1$, well above any of our frequencies of interest in the sound field.

A.3 Source Decomposition

Neglecting viscosity, Lighthill's noise source is the double divergence of $T_{ij} = \rho u_i u_j + (p - a_\infty^2 \rho)\delta_{ij}$, where u_i are the instantaneous velocities, and p and ρ are the instantaneous pressure and density. The source decomposition we consider splits T_{ij} into components that are linear, T_{ij}^l, and quadratic, T_{ij}^n, in velocity fluctuations plus the so-named entropy component, T_{ij}^s:

$$T_{ij} = \underbrace{\rho\bar{u}_i\bar{u}_j + (\bar{p} - a_\infty^2\bar{\rho})}_{T_{ij}^m} + \underbrace{\rho\bar{u}_i u_j' + \rho\bar{u}_j u_i'}_{T_{ij}^l} + \underbrace{\rho u_i' u_j'}_{T_{ij}^n} + \underbrace{(p' - a_\infty^2\rho')\delta_{ij}}_{T_{ij}^s}. \tag{3}$$

α	T_{ij} (5)	T_{ij} (11)	$T^{\bar{\rho}}{}_{ij}$ (5)	$T^{n}{}_{ij}$ (5)	$T^{n}{}_{ij}$ (11)
30.00	30.45	30.74	31.81	21.45	21.65
60.00	11.00	11.33	11.32	11.14	11.35
90.00	5.66	5.99	5.84	4.93	5.10
120.00	2.99	3.09	3.17	1.56	1.61

Table 1: Evaluation of use of $\rho u_i u_j$ for $\bar{\rho} u_i u_j$ and truncation of azimuthal Fourier series expansion. Values shown are $\overline{p'p'}/\rho_j^2 U_j^4 \times 10^{10}$ on a circular arc at $240 r_o$. The numbers in parenthesis, (5) and (11), are $N_{n_{\max}}$.

The mean component T_{ij}^m by definition does not make noise. We have not decomposed the density as one might into $\rho = \bar{\rho} + \rho'$ in the velocity terms, because, as seen in table 1, the sound from T_{ij} is nearly the same as that from

$$T_{ij}^{\bar{\rho}} = \bar{\rho} u_i u_j + (p' - a_\infty^2 \rho') \delta_{ij}. \tag{4}$$

Thus we do not discuss the explicit effect of density fluctuations in the $\rho u_i u_j$ terms.

In the spirit of Lighthill's pioneering work,[12,21] Ribner[6] made extensive use of this source decomposition. More recently this decomposition has been coupled to k–ε turbulence models as a predictive tool.[22,23] A similar decomposition into self-noise and shear noise components is also used in modeling the source terms[7,8,10,24] in the linearized Lilley equation,[14] which extends the acoustic analogy approach to explicitly include refraction.

A.4 Computing the Far-Field Sound

Given T_{ij} or one of its components, the following procedure was used to compute the far-field sound. The data were first transformed in θ by

$$\tilde{T}_{ij}^{(n)}(x, r, t) = \frac{1}{N_\theta} \sum_{k=0}^{N_\theta - 1} T_{ij}(x, r, \theta_k, t) e^{in\theta_k} \qquad \text{for} \quad n = -N_{n_{\max}}, \ldots, N_{n_{\max}}, \tag{5}$$

which was done as an efficient and accurate means of compressing the data. The stress tensor T_{ij} was rotated into cylindrical coordinates to facilitate the transform. We see in table 1 that the noise eventually computed from $N_{n_{\max}} = 5$ versus $N_{n_{\max}} = 11$ modes differs little, so we take $N_{n_{\max}} = 5$ as sufficient.

Next, $\tilde{T}_{ij}^{(n)}(x, r, t)$ was transformed in time following a procedure similar to that we used in the past.[2] The time series at each x and r mesh point and n-mode was first multiplied by

$$w(t) = \frac{1}{2}\left[\tanh\left(5\frac{t - t_1}{t_1 - t_0}\right) - \tanh\left(5\frac{t_f - t}{t_f - t_2}\right)\right], \tag{6}$$

where t_0 and t_f in (6) are the times in the simulation when it was determined to be statistically stationary and the final time, respectively. Times t_1 and t_2 are the 5 and 95 percent points in this time series. This contaminates the resulting noise, but only for a finite length of time that can be unambiguously identified in advance through straight forward retarded time considerations. The time transform was then

$$\check{T}_{ij}^{(n)}(x, r, \omega_m) = \frac{1}{N_t} \sum_{l=1}^{N_t} w(t_l) \tilde{T}_{ij}^{(n)}(x, r, t_l) e^{-i\omega_m t_l} \qquad \text{for} \quad m = -N_t/2, \ldots, N_t/2 - 1, \tag{7}$$

where $N_t = 2304$, and the discrete angular frequencies were defined $\omega_m = 2\pi m/T$, where T is the implied time period.

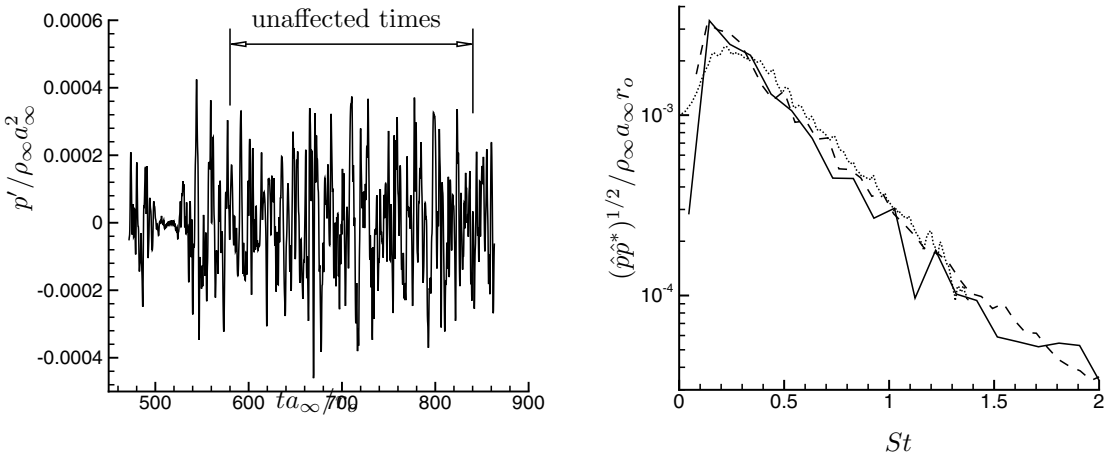

Figure 6: Sound data at $\alpha = 30°$, $60r_o$ from the nozzle. (a) Time history shows region affected by the windowing procedure. (b) Time spectra: —— present solution of the Lighthill equation, - - - - from Freund,[2] and ····· from the experiment of Stromberg *et al.*[1] Only a relative scale was provided by Stromberg *et al.* so it has been adjusted vertically.

Finally, the data were inverse transformed in θ by

$$\hat{T}_{ij}(x, r, \theta_k, \omega_m) = \sum_{n=-N_{\theta_{\max}}}^{N_{\theta_{\max}}} \check{T}_{ij}^{(n)}(x, r, \omega_m) e^{in\theta_k} \qquad \text{for} \quad k = 0, \ldots, N_\theta - 1, \tag{8}$$

rotated into Cartesian coordinates, and convolved with the twice differentiated free-space Green's function for the Helmholtz equation to compute the acoustic pressure Fourier coefficients $\hat{p}'(\mathbf{x}, \omega_m)$ at listener point $\mathbf{x}$,

$$\hat{p}'(\mathbf{x}, \omega_m) = \int_\Omega \hat{T}_{ij}(\mathbf{y}, \omega_m) \frac{\partial^2}{\partial x_i \partial x_j} \left[\frac{e^{-i\omega_m |\mathbf{x}-\mathbf{y}|/a_\infty}}{4\pi |\mathbf{x}-\mathbf{y}|} \right] d\mathbf{y} \qquad \text{for} \quad m = -N_{\omega_{\max}}, \ldots, N_{\omega_{\max}}, \tag{9}$$

where we have used $\hat{p}' = a_\infty^2 \hat{\rho}'$. Ω is the physically realistic region of the cylindrical simulation domain, which extended $x = 31r_o$ downstream from the nozzle and out to $r = 8r_o$. Taking $N_{\omega_{\max}} = 327$ was sufficient to compute all frequencies up to $St = 2.0$, a range which, as we shall see, constitutes most of the noise from this jet. The time dependent pressure at point $\mathbf{x}$ is

$$p'(\mathbf{x}, t_l) = \sum_{m=-N_{\omega_{\max}}}^{N_{\omega_{\max}}} \hat{p}'(\mathbf{x}, \omega_m) e^{-i\omega_m t_l} \qquad \text{for} \quad l = 0, \ldots, N_t - 1. \tag{10}$$

Figure 6 (a) shows $p(\mathbf{x}, t)$ at 30° from the jet axis and $60r_o$ from the nozzle. The region affected by the 'windowing' procedure is evident, but constitutes less than one-quarter of the time series. There are sufficient unaffected data to converge statistics. Figure 6 (b) shows the energy spectrum of the pressure fluctuations at this same point, comparing with corresponding experimental data and the spectrum at the same position computed previously using a different method.

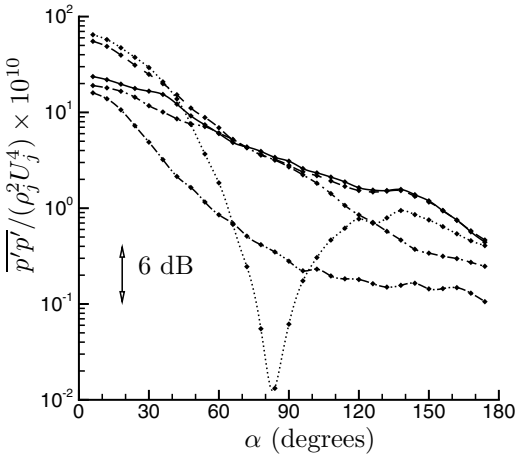

Figure 7: Directivity on a circular arc $240r_o$ from the nozzle: —— T_{ij}; - - - - $T_{ij} - T_{ij}^s$; ····· using T_{ij}^l; —·— T_{ij}^n; and —··— T_{ij}^s, as defined in (3).

A.5 Directivity

Figure 7 shows that the sound from the shear noise source, T_{ij}^l, is more directional than the self-noise source, T_{ij}^n, and has an angle of extinction near $\alpha = 90°$. The entropic term is highly directional at small angles, but has nearly uniform directivity for $\alpha \gtrsim 90°$. While the T_{ij}^s term is indeed insubstantial at large angles, near to the downstream jet axis it is significant even though the temperature ratio of this jet is only $T_j/T_\infty = 0.86$. Mitchell *et al.*[25] also found this term to be non-negligible for the noise from vortex pairing in an truly (not just in the mean) axisymmetric uniform temperature jet. This is surprising since, as expected, $\overline{(p' - a_\infty^2\rho')^2}$ is small compared to the Reynolds stresses: $\overline{(p' - a_\infty^2\rho')^2}_{\max} = 0.0062\rho_j^2 U_j^4$, whereas the Reynolds stresses have peaks of $\overline{u_x'u_x'}_{\max} \approx 0.040U_j^2$ and $\overline{u_r'u_r'}_{r\max} \approx 0.023U_j^2$, for example.

Lilley[26] finds it instuctive to rewrite the $p - a_\infty^2\rho$ term in terms of the fluctuating total enthalpy and a kinetic energy component. Using the energy equation and the perfect gas equation of state, it is equivalent to

$$p - a_\infty^2\rho = \underbrace{-\frac{\gamma-1}{2}\rho u^2}_{\text{term I}} + \underbrace{a_\infty^2 \int \frac{\partial}{\partial x_j}\left[\rho u_j\left(\frac{h_\infty - h_s}{h_\infty}\right)\right] dt}_{\text{term II}}. \tag{11}$$

Lilley shows that the second (II) term has a dipole form and is hence more acoustically efficient and suggests that it explains the less-than-U^8 sound power scaling of hot jets. Here we find that it is much larger than term I and constitues most of the $p - a_\infty^2\rho$ term's contribution to the far-field sound.

The net acoustic power (all angles) of the different components is tabulated in table 2. We see that the power from just quadratic velocity fluctuations terms is 83 percent of the total, which suggests that a large part of the apparent acoustic energy due to T_{ij}^l can, in fact, potentially be interpreted as redirection due by flow-acoustic interaction.

None of the profiles show a decrease in intensity near to the jet axis, as might be expected due to refraction, but a zone of 'silence' is not expected for the total for the frequencies in this jet (*e.g.* Lush[27]). If we divide the data into higher and lower frequency components, we see the expected behavior (figure 9). (We cannot analyze band-limited spectral components like Lush since we do not have sufficient date to converge statistics in frequency bands.) Low frequencies

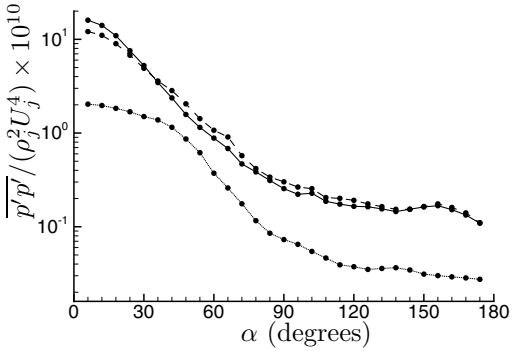

Figure 8: Directivity on a circular arc $240r_o$ from the nozzle: —— $p - a_\infty^2\rho$; ---- term I in 11; and ····· term II in 11.

Component	Power/$\rho_j {U_j}^3 A_j$	Power/Power T_{ij}
T_{ij}	8.3 $\times 10^{-5}$	1.00
T_{ij}^l	8.7 $\times 10^{-5}$	1.05
T_{ij}^n	6.9 $\times 10^{-5}$	0.83
T_{ij}^s	2.0 $\times 10^{-5}$	0.25

Table 2: Net radiated acoustic power.

are more intense along the axis, which Goldstein[28] suggests is a low-frequency flow acoustic interaction, and high-frequency noise is reduced near the jet axis, as expected for refraction. So there is significant evidence of refraction, but we note that since the source is only evaluated for $x < 31r_o$ any refraction down stream of this point is omitted, though this omitted part is likely to be less substantial since the Mach number is substantially decreased here.

It is clear that some individual components are more intense than the total, which means that the noise from the different components is correlated, significantly so given the amount of cancellation evident in figure 7. Taking $T_{ij} \approx \bar{\rho} u_i u_j$, Goldstein & Rosenbaum[29] show that a sufficient condition to decorrelate the shear noise and self-noise is that the jet turbulence be locally homogeneous. To quantify the observed correlation, we define a correlation coefficient as

$$C_{\beta-\gamma} = \frac{\overline{\rho^\beta \rho^\gamma}}{\rho_{\rm rms}^\beta \rho_{\rm rms}^\gamma}, \tag{12}$$

where β and γ are n, l, or s to indicate the noise from different source contributions defined in (3). C_{l-s}, C_{l-n}, and C_{n-s} are plotted in figure 10. All pairs are most correlated at small angles and for the most part are canceling. At very small angles, the entropic contribution cancels the noise due to T_{ij}^l with correlation coefficient $C_{l-s} \approx -0.6$. Some degree of correlation has been deduced from experimental observations of hot supersonic jets,[30] but it does not appear to have been anticipated to this degree for a nearly uniform temperature subsonic jet. The linear and quadratic velocity fluctuation contributions are also correlated at small angles, though they are often assumed to be decorrelated in models.[6,7,22] The noise from source components that are quadratic in the velocity fluctuations are relatively mildly correlated with the entropic noise. All correlations decrease to near zero by $\alpha = 90°$.

Ribner[6] predicted that five inverse Doppler factors[31] would set the directivity of the velocity components of the source, with an additional factor of $\cos^4\alpha + \cos^2\alpha$ for the T_{ij}^l component.

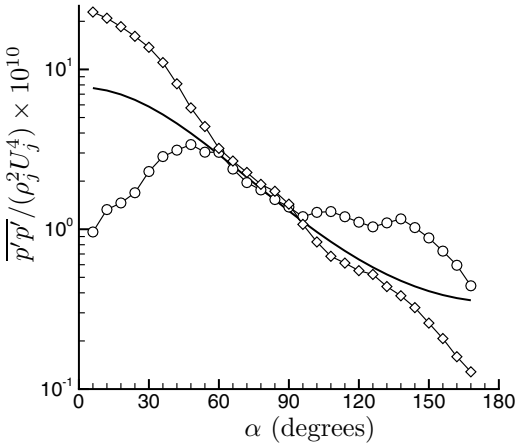

Figure 9: Directivity for high and low frequencies: $\circ$ $St < 0.45(1 - M_c \cos\alpha)^{-1}$; $\diamond$ $St > 0.45(1 - M_c \cos\alpha)^{-1}$. The —— line is $(1 - M_c \cos\alpha)^{-5}$ with $M_c = 0.3$ suggested as suggested by direct analysis of $T_{ij,ij}$.[2]

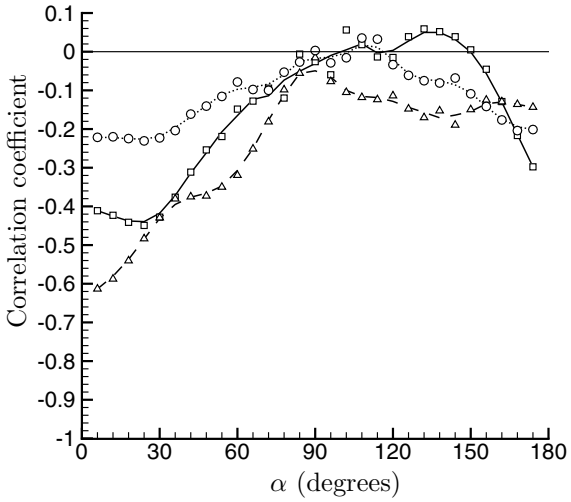

Figure 10: Correlation coefficients defined by (12): $\square$ C_{l-n} with smoothed profile —— ; $\triangle$ C_{l-s} with smoothed profile - - - - ; and $\circ$ with smoothed profile ····· .

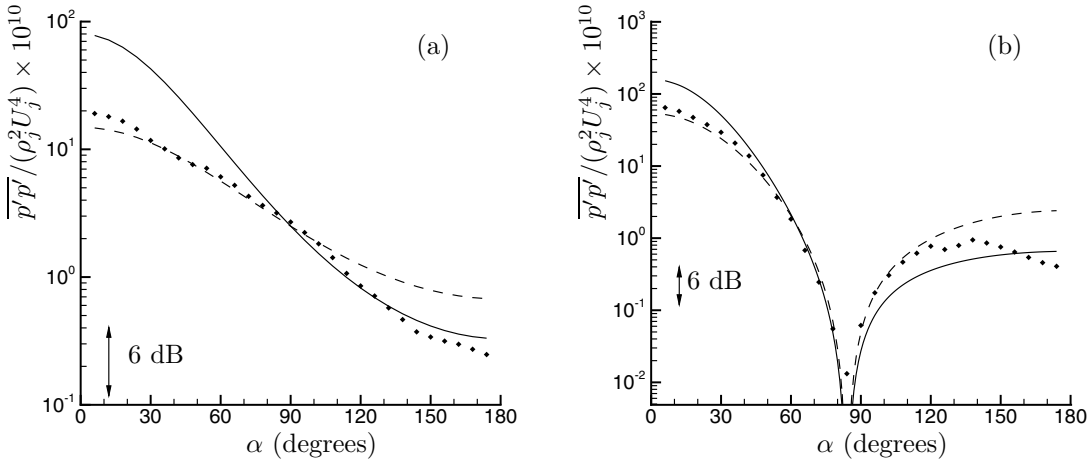

Figure 11: Directivity on a circular arc $240r_o$ from the nozzle. (a) • T_{ij}^n, —— $2.5(1-0.5\cos\alpha)^{-5}$, ---- $2.5(1-0.3\cos\alpha)^{-5}$; (b) • T_{ij}^l, —— $2.5(\cos^4\beta+\cos^2\beta)(1-0.5\cos\alpha)^{-5}$, ---- $4.5(\cos^4\beta+\cos^2\beta)(1-0.3\cos\alpha)^{-5}$. Angle β is defined based on an origin at $x=20r_o$, which is presumably closer the center of the apparent source location.

Figure 11 (a) shows the self-noise component. It is significantly less directional than five inverse Doppler factors would have it with $M_c \equiv U_c/a_\infty = 0.6U_j/a_\infty = 0.5$. However, Freund[2] showed that the wave-number/frequency makeup of the full Lighthill source for this jet had a dominate phase Mach number of $M_c \approx 0.3$, which is indeed a better fit for the data. Accounting for refraction by the mean flow in the high-frequency limit, Goldstein shows that three inverse Doppler factors are actually to be expected, which is also closer to what is observed than five Doppler factors, but since the mean velocity profile does not appear in the solution for the source T_{ij}^n interactions with the mean flow leading to refraction are not a viable explanation in this particular case. A possibility is that the emitted directivity of five inverse Doppler factors is made more uniform by interaction with turbulence rather than the mean, which would be included as an artificial source in T_{ij}^n. Such a change of directivity has been suggested based on qualitative analysis of this database,[32] but has not been demonstrated quantitatively for the frequencies and source locations present. For the shear noise, the observed angle of extinction matches well with Ribner's theory if the effective source location is shifted to $x = 20r_o$ (figure 11 b). Again, $M_c = 0.3$ yields a better fit than $M_c = 0.5$. Ribner[6] predicted that the shear noise would be 3dB higher than the self-noise on axis, but we observe nearly 6dB difference. Nonetheless, the agreement is encouraging.

A.6 Quadrupole character

The approach taken to solve for the far-field noise described in section A.4, specifically the choice of convolving T_{ij} with the twice-differentiated Green's function $G_{,ij}$ for the free-space homogeneous reduced wave equation, was made to reduce numerical errors. The $T_{ij} * G_{,ij}$ is mathematically equivalent, of course, to a convolution of the double-divergence of the stress with just G: $T_{ij,ij} * G$. However, based on Lighthill's theory, we anticipated that the noise sources should have quadrupole character. The approach taken implicity includes cancellation that would lead to effectively quadrupole type source, whereas the $T_{ij,ij} * G$ method would have challenged the fidelty of the differentiaion of T_{ij} and the quadrature to accurately represent these cancellation in the numerics. Indeed, we were not able to successfully compute the far-

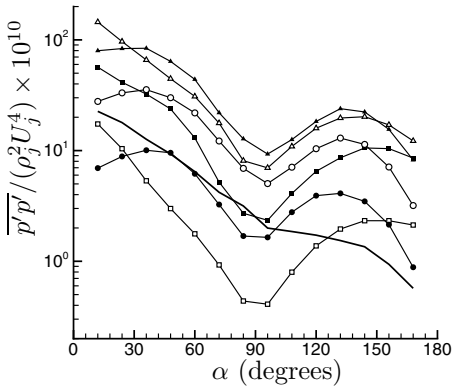

Figure 12: The effecive directivity of streamwise portions of the jet as defined by dividing (9) into sub-inetegral in x: $0 \le x \le 5r_o$ □ ; $5r_o \le x < 10r_o$ ■ ; $10r_o \le x < 15r_o$ △ ; $15r_o \le x < 20r_o$ ▲ ; $20r_o \le x < 25r_o$; and $25r_o \le x < 30r_o$. The ——line is the total.

field noise by summing up the monopoles directly. (The principal difficulty appeared to be in the accuate computation double-divergence operation on the reduced every-other-mesh-point mesh.) Taking this selected approach, we find negligible sensitivity to how the downstream and upstream boundaries are treated, in contrast to the Lighthill solution of Mitchell *et al.*,[33] and good agreement with other methods for computing the far-field noise from this simulation.[2] This success suggests that quadrupole-like cancelation are important, but we can not conclude directly that the noise is quadruopole, or even if it is well modeled by quadrupoles.

It is difficult to attach a particular noise source type label to jet turbulence because it is a distributed source, whereas the term 'quadrupole' itself is best defined for a point source. Lighthill himself points out[34] that treatment of finite Mach number jets by his theory is an extrapolation of a $M \to 0$ theory and therefore subject to the standard caveats.

We can make an indirect test of whether the source is close to a distribution of point quadrupoles by computing the noise from a part of the jet. If the noise depends only on quadrupole cancellations, the noise from any part of the jet should be less than the total and we could then add up the directivity of different components without worry of missing cancellation. This would be attractive from a modeling perspective because it would allow us to define the noise from a part of the jet, for example a particular streamwise slice. However, if non-quadrupole cancellation are substantial, we will be able within this approach not be able to make such a definition.

Figure 12 show that the noise from downstream chunks of the jet is actually much louder than the total. There are substantial non-quadrupole cancellation that are disrupted when the integral (9) is split in x. The total of course matches exactly by the nature of the numerical quadrature, but the mean-square pressure directivities are individually far too loud. This is congruous with different observations made in a previous study of this database which suggested a non-quadrupole character for the sources.[2] Within Lighthill's theory it does not seem possible to define the noise from a downstream region in a jet, though this does not substantial the potential facility of models build on such an assumption. [check Lilly JSV paper]

A.7 Time spectra

All the components contribute to the far-field sound over a range of frequencies, but their spectral shapes differ for different components and, for some, are strongly dependent on α. Figure 13 shows far-field noise spectra at four different angles. Closest to the jet at $\alpha = 30°$

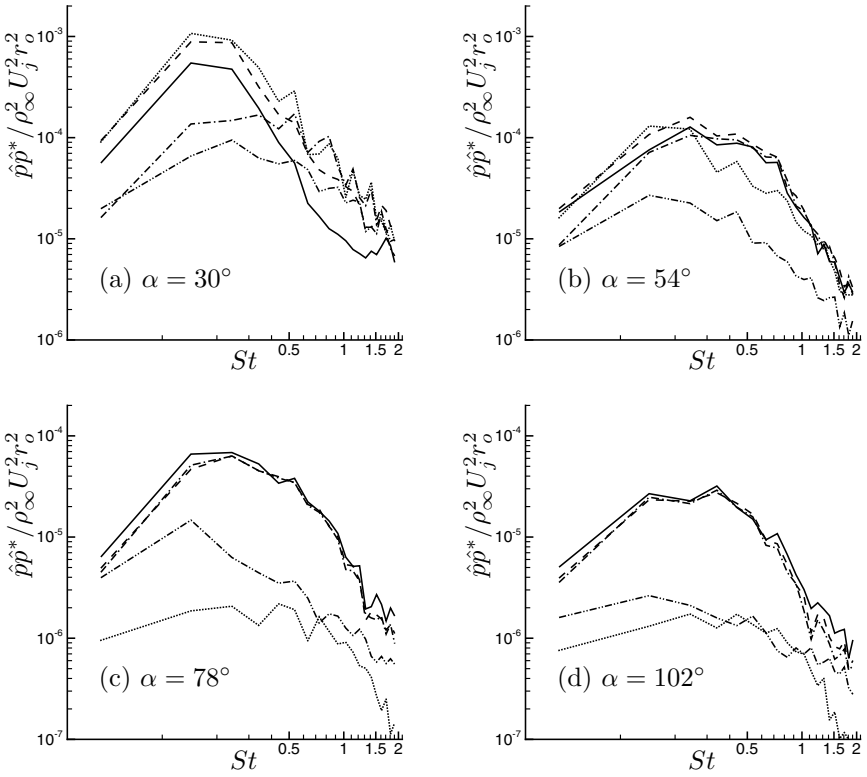

Figure 13: Pressure spectra: —— T_{ij} total; - - - - $T^l_{ij} + T^n_{ij}$ all velocity terms; ····· T^l_{ij} velocity terms linear in fluctuations; —·— T^n_{ij} velocity terms nonlinear in fluctuations; —··— T^s_{ij} entropy term.

(figure 13 a), the low frequency noise is primarily due to T^l_{ij}. The noise from just T^s_{ij} is small here, but because it is so highly anti-correlated with that from T^l_{ij} it cancels a portion of the T^l_{ij} noise. By itself, the noise from T^n_{ij} at higher frequencies is comparable to that just from T^l_{ij}. At $\alpha = 54°$ (figure 13 b), the noise from T^l_{ij} makes of the greater part of the total noise for $St < 0.3$ (though still somewhat canceled by the noise from T^s_{ij}) whereas the noise from T^n_{ij} is more significant for $St > 0.3$. Both have similar levels for $St \gtrsim 0.8$. At $\alpha = 78°$ and $102°$ (figures 13 c and d), the noise from T^n_{ij} and T_{ij} are essentially the same.

Figure 14 illustrates how the spectral shape of the different components change with α. The spectrum from the full source T_{ij} clearly becomes broader with increasing α (figure 14 a). However, the spectral shape of the noise from T^n_{ij} is relatively unchanged (figure 14 c). It is the change in shape of the spectrum from T^l_{ij} and its rapidly decreasing significance near $\alpha = 90°$ (figure 14 b) that account for most of the change of the full spectrum. The spectral peak of the noise from just T^s_{ij} (figure 14 d) shifts to lower frequencies (from $St \approx 0.35$ to $St \approx 0.15$), but its shape is relatively broad and otherwise insensitive to α. The shifts follows to the Doppler factor $(1 - M_c \cos\alpha)$ with M_c now equal to $0.6U_j/a_\infty = 0.5$ (figure 15). This is surprising since we saw in the previous section that the directivity was better fitted using $M_c = 0.3$. It seems that this most intense frequency comes from the structures convecting near the end of the potential core, as suggested by visualizations.[2] This is where M_c should be closest to $0.6U_j/a_\infty$.

Tam[35] suggests that jet noise spectra are composed of two distinct components: one due to large-scale structures and one due to fine-grained turbulence. Here we see that the sound from T^n_{ij} is similar to Tam's nominal fine-grained turbulence contributions, while that from T^l_{ij}, being

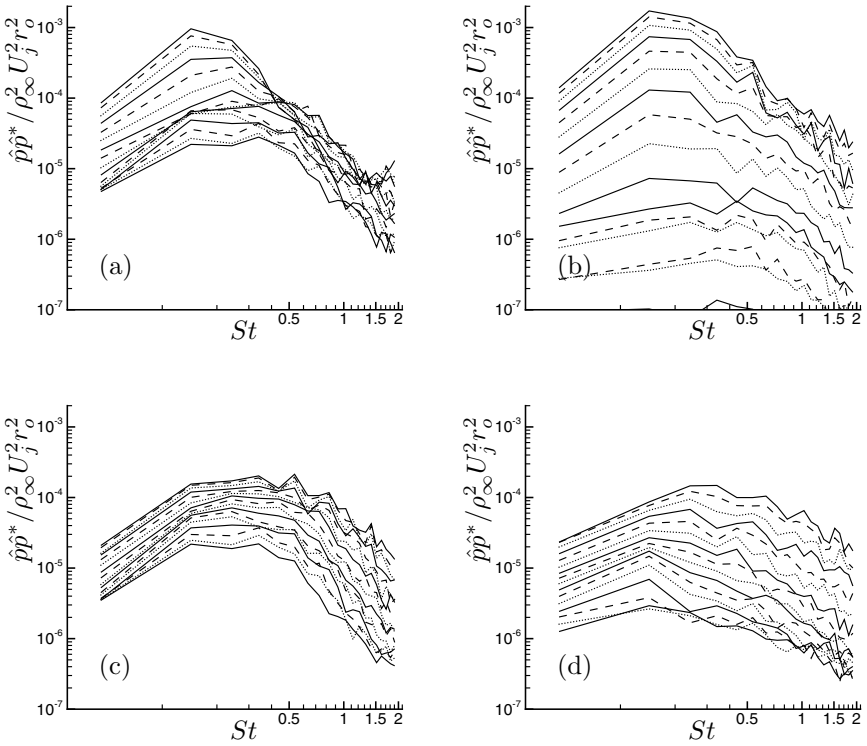

Figure 14: Pressure spectra: (a) T_{ij} all components; (b) T_{ij}^l components linear in velocity fluctuations; (c) T_{ij}^n components quadratic in velocity fluctuations; (d) T_{ij}^s 'entropic' component. Spectra at every 6° form $\alpha = 18°$ (top curve) to $\alpha = 102°$ (bottom curve) are shown.

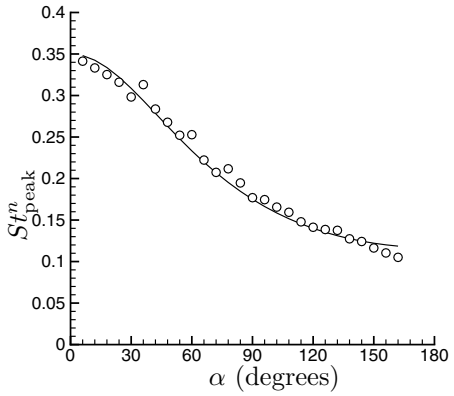

Figure 15: Peak Strouhal number due directly to T_{ij}^n: ∘ from simulation; —— $0.175(1-M_c\cos\alpha)^{-1}$ with $M_c = 0.6U_j/a_\infty$. The peak was determined by fitting third-order polynomials to the spectra in log-log coordinates. This removed statistical variations and provided an unambiguous recipe for determining the peak.

more peaked at lower frequencies, is qualitatively similar to his nominal large-scale contribution. Unfortunately, the present jet has a Reynolds number dependent spectrum so direct comparison with Tam's empirical spectra is not instructive. However, the shear noise/self-noise decomposition is an artifact of the Reynolds average, which is made for modeling convenience, though it does seem to also divide the radiated noise into a part whose spectrum varies substantially with angle and a part that does not. But it does this without a formal splitting of the scales since all velocity fluctuations participate in both the shear noise and self-noise sources. The empirical predictive tool of Tam & Auriault[36] for the noise near $\alpha = 90^\circ$ might be assisted by the fact the noise is, in a sense, simpler here, not depending on the mean flow through T_{ij}^l and having no substantial 'entropic' contribution.

A.8 Noise source statistics

Making a compact source assumption, the radiated acoustic intensity is directly related to the volume integral of the of the space/retarded-time covariance of the Lighthill stress,

$$I(\mathbf{x}) = \frac{x_i x_j x_k x_l}{16\pi^2 a_\infty^5 |\mathbf{x}|^5} \times \int_\infty \int_\infty \frac{\partial^4}{\partial \tau^4} \overline{T_{ij}(\mathbf{y},t) T_{kl}(\mathbf{y}+\boldsymbol{\xi}, t+\tau)}\, d\boldsymbol{\xi}\, d\mathbf{y}, \tag{13}$$

which follows after Lighthill[12] and Ffowcs Williams[31] and was used extensively by Ribner.[6] Often in formulating statistical noise models, the stress tensors are approximated as[6]

$$T_{ij} \approx \rho u_i u_j, \tag{14}$$

which gives the sound due to a point in the flow as

$$I_{ijkl}^p \propto \frac{\partial^4}{\partial \tau^4} \int_\infty \overline{u_i u_j u_k' u_l'}\, d\boldsymbol{\xi}, \tag{15}$$

a formula that is the basis of some modern statistical jet noise models.[7,17] We have seen that the $(p - a_\infty^2 \rho)$ term, which is neglected here, does indeed alter the directivity, but mostly near the jet axis. It does not contribute much to the net radiated power (table 2) or for $\alpha \gtrsim 45^\circ$.

The fourth-order integrated space/retarded-time correlation (15) that constitutes the core of (13) is often simplified to facilitate the use of experimental data in tunning models. Assuming that the turbulence has a normal joint probability distribution gives[37]

$$R_{ijkl} = \overline{u_i u_j u_k' u_l'} = \overline{u_i u_j}\ \overline{u_k' u_l'} + \overline{u_i u_k'}\ \overline{u_j u_l'} + \overline{u_i u_l'}\ \overline{u_j u_k'}. \tag{16}$$

This is checked directly in figure 17 for the normal components at the points indicated in figure 16. Though convergence is relative poor for the fourth-order tensor, the agreement is seen to be very good, justifying the approximation in (16). Other components are more difficult to converge when computed as the fourth-order correlation because the τ-dependent component, $\overline{u_i u_k'}\ \overline{u_j u_l'} + \overline{u_i u_l'}\ \overline{u_j u_k'}$, is relatively smaller compared to the τ-independent component and are not shown. Nevertheless, our results suggest that two-point correlation statistics, which are relatively easy to measure at least in one direction, can be used in (16), a generalization of which has been provided by Lighthill.[19] Two-point correlations are known to be well-fitted by exponential functions in high-Reynolds-number jets,[38] but not necessarily in low-Reynolds-number simulations of homogeneous turbulence, as discussed in the context of noise by Lilley.[39] Thus it is important to check their form here in our low-Reynolds-number jet. Figure 18 shows $\overline{v_x(x_o) v_x(x_o + \xi)}$ for $x_o = 18.0 r_o$ and $x_o = 26.5 r_o$, both at $r = r_o$, and fitted by exponential functions. The fits are good, essentially perfect at $x = 26.5 r_o$ where the local Reynolds number is, of course, higher. Likewise, the temporal two-point correlations are strongly peaked and also well fitted by exponentials (figure 19).

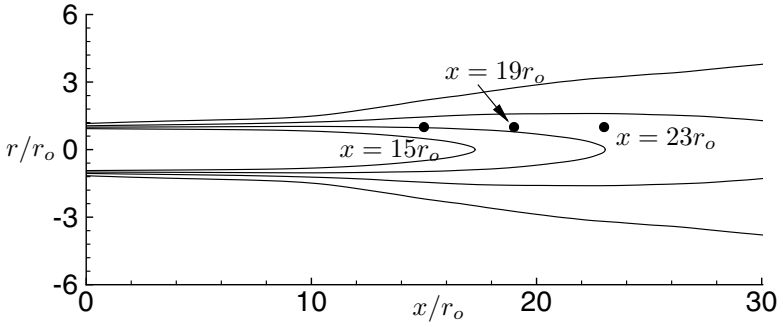

Figure 16: Schematic showing points used relative to mean velocity. All are coincident with the nozzle lip at $r = r_o$.

x/r_o	$ijkl$	E_2	$\tau_o a_\infty / r_o$
15	1111	0.015	3.851
	1212	0.021	4.113
	2222	0.042	2.595
	3333	0.019	2.573
19	1111	0.028	4.379
	1212	0.025	4.809
	2222	0.032	2.866
	3333	0.022	2.690
23	1111	0.048	6.131
	1212	0.021	6.763
	2222	0.024	3.461
	3333	0.019	3.307

Table 3: Parameters for fitting with (18). E_2 is the error norm for the fit: $E_2 = r_o^{-1} a_\infty \int (f - P/P_{\max})^2 \, d\tau$.

Of course, the acoustic intensity (13) depends upon the integrated correlation,

$$P_{ijkl} = \int_\infty \overline{u_i u_j u'_k u'_l} \, d\boldsymbol{\xi}, \tag{17}$$

which, based on two-point correlations, is often assumed to also have an exponential form.[7,9] However, this is not the case as seen in figure (20) where it is instead well-fitted by Gaussian functions,

$$f(\tau) = \exp\left[\frac{\tau^2}{\tau_o^2}\right], \tag{18}$$

despite the good exponential function fits of the one-dimensional two point in time correlations. Data at $x = 19r_o$, $r = 1.1r_o$ are plotted in figure 17 and the fitting coefficients for all points in are given in table 3. As seen by the error norms given in this table, all the fits are very good. We also see that the width of the Gaussian depends on the components, with the same relative widths at the different x-points. To compute noise, this data is differenced in time four times, so even the small deviation from Gaussian that we see in figure 17 will potentially be important. Nevertheless, error for using an exponential fit for this flow would be much greater.

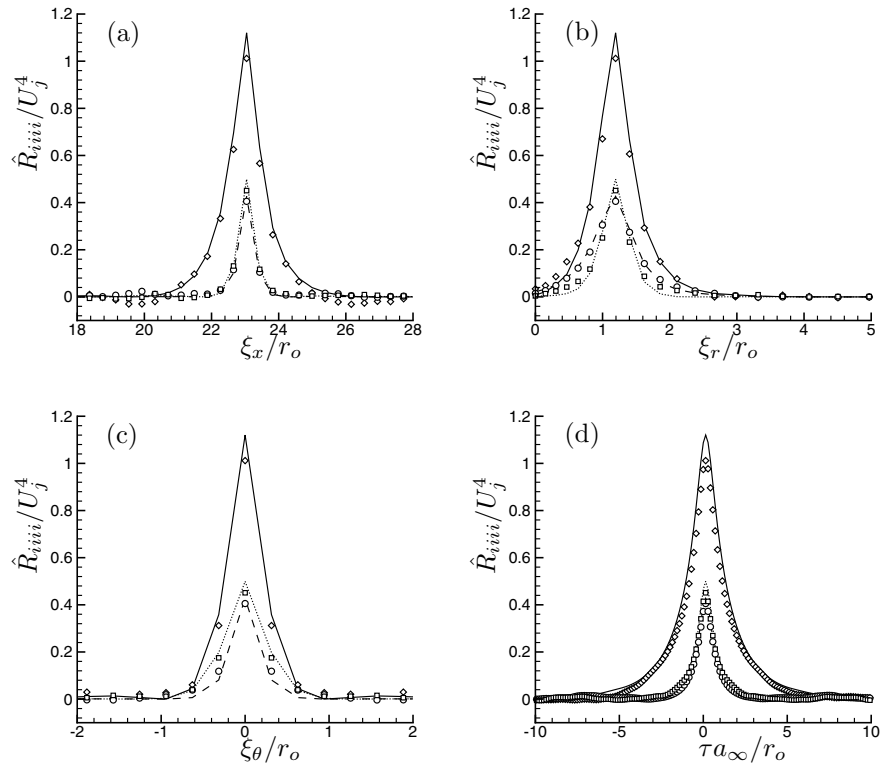

Figure 17: Direct evaluation of (16) for normal components at $x = 23r_o$ and $r = 1.1r_o$. The lines are $\hat{R}_{iiii} = \overline{u_i u_i'}\ \overline{u_i u_i'} + \overline{u_i u_i'}\ \overline{u_i u_i'}$ and the symbols are $\hat{R}_{iiii} = \overline{u_i u_i u_i' u_i'} - \overline{u_i u_i}\ \overline{u_i' u_i'}$: —— and ◇ are 1111, - - - - and ○ are 2222, and ····· and □ are 3333. One dimensional offsets in (a) ξ_x, (b) ξ_r, (c) ξ_θ, and (d) τ.

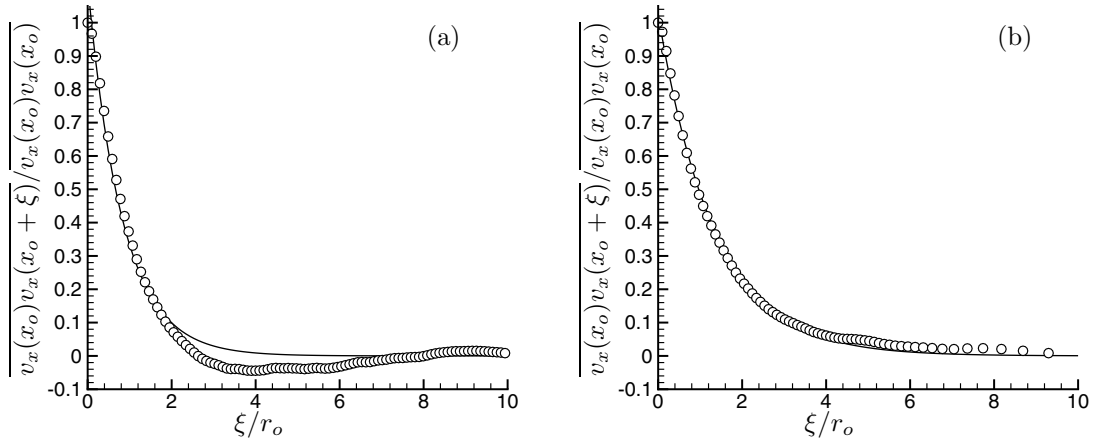

Figure 18: Axial two-point correlation for (a) $x_o = 19r_o$ and (b) $x_o = 26.5r_o$ with exponential fits $\exp(-x/0.83)$ and $\exp(-x/1.34)$, respectively.

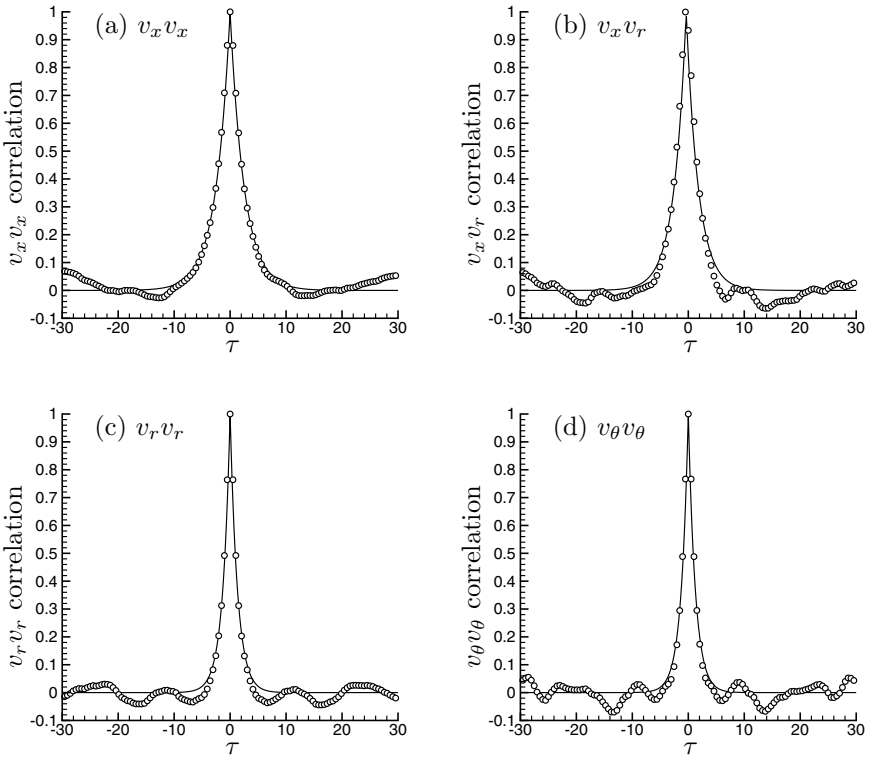

Figure 19: Two point in time correlations, $\overline{v(t)v(t+\tau)}$, at $r = 1.1r_o$ and $x = 19r_o$. The —— lines are exponential fits by $\exp(-\tau/\tau_o)$: (a) $v_x v_x$ with $\tau_o = 2.54$, (b) $v_x v_r$ with $\tau_o = 2.18$, (c) $v_r v_r$ with $\tau_o = 1.32$, (b) $v_\theta v_\theta$ with $\tau_o = 1.27$.

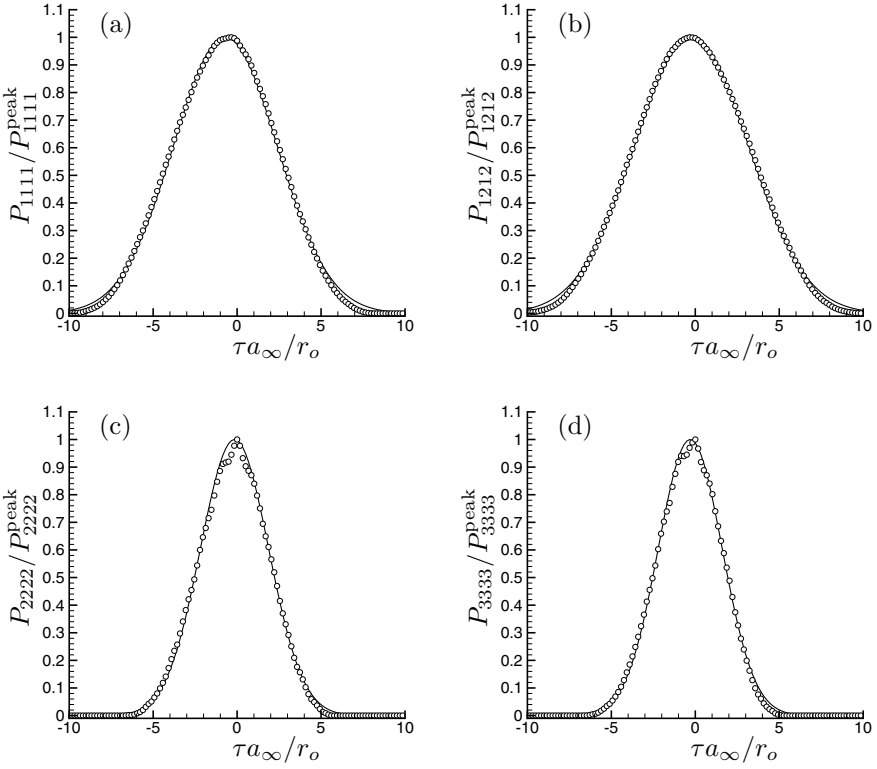

Figure 20: Integrated fourth-order correlation tensor as defined in (17) shown with open circles ∘ and Gaussian fits —— . Fitting parameters are given in table 3.

A.9 Conclusions and closing

The implications for modeling using shear noise, self-noise, and 'entropic' source decompositions are clear. These contributions are highly correlated at small angles to the jet, not statistically independent as often assumed. Ribner's theory, though qualitatively correct in predicting the individual contributions of the shear noise and self-noise, especially if $M_c = 0.3$ is used to reflect the computed dominant phase velocity of T_{ij} for this jet, but will miss their substantial mutual cancellation. Several more recent models, which have followed this same philosophy, also omit shear noise/self-noise correlation. An implication of this conclusion is that locally homogeneous turbulence, which is sufficient to decorrelate the shear noise and self-noise,[29] may not be an acceptable model for the noise source, at least at small angles to the downstream axis.

Even for this nearly uniform temperature jet, the entropic source's contribution to the far-field noise is important at small angles, especially due to its high correlation with the shear noise. Neglecting it leads to a substantial over prediction of the far-field sound. The present jet with $U_j/a_\infty = 0.83$ is close to the point where the experiments of Tanna[40] show the least sensitivity to jet temperature, so we can anticipate that this will become more significant at substantially higher or lower jet velocities.

The sideline noise is dominated by terms in the Lighthill source that are independent of the mean flow and entropic terms. This should greatly simplify modeling for this portion of the radiated sound, perhaps making it more amenable to empirical fits.

We find that downstream of the potential core's closing two-point correlations are well fitted by exponential functions, which is characteristic of high-Reynolds-number turbulent flows. (In the laminar/transitional shear layers they are more similar to the wavy correlations expected for flows dominated by instability waves, as expected in this region at $Re = 3600$.[2]) The fourth-order space/retarded-time covariance tensors, which are more directly related to the far-field sound, are well approximated by the standard simplification into products of second-order correlations, which assume a normal distribution for the turbulence. However, despite the good exponential fits of the one-dimensional components, the volume integrated fourth-order correlation tensor is very well fitted by Gaussian functions, of different widths for different components. Both its form and dependence on components are counter to standard modeling procedures.

It seems appropriate in closing to make a final comment concerning the Reynolds number of the simulation used, which is low for a turbulent jet by every standard aside from modern direct numerical simulation capabilities. It is conceivable that the correlations that we observe might be an artifact of this low Reynolds number, but they are so significant that it seems unlikely that they could disappear altogether at higher Reynolds numbers. Once turbulent, the Reynolds stresses are in close agreement to jets of much higher Reynolds numbers and the two-point correlations decay rapidly, just as at higher Reynolds numbers.[2] It does not seem feasible that the energetic structures could change sufficiently with Reynolds number to display a behavior much different than we observe. What will certainly change at higher Reynolds numbers is that the near-nozzle shear layers will become turbulent. Since these eddies are relatively small, we can anticipate that they will make the high-frequency noise missing from the present simulation. Unfortunately, there does not appear to be a definitive means of directly testing these admittedly speculative assertions: we have pressed the limit of direct numerical simulation* and experimentalists have pressed the limits of their measurement techniques. Further technological advances in both might facilitate a better parameterization of Reynolds number effects in the future and at the same time allow the details of high-Reynolds-number jet noise sources to be probed in detail as we have done here in the low-Reynolds-number limit.

*Large-eddy simulation is promising, but seems to have a resolution requirement for a high-Reynolds-number jet that is greater than the present direct numerical simulation.[41]

Acknowledgments

The author acknowledges the assistance of Devon Johnson in identifying the approach used to compute the far-field sound. He also thanks Prof. Tim Colonius for making critical comments on a early draft of this paper. Financial support from NASA is gratefully acknowledged.

B Ray Traces Through Unsteady Jet Turbulence

J. B. Freund
Theoretical and Applied Mechanics
University of Illinois at Urbana-Champaign
T. G. Fleischman
Mechanical and Aerospace Engineering
University of California, Los Angeles

B.1 Abstract

Results of an ongoing effort to quantify the role turbulence in scattering sound in jets are reported. Using a direct numerical simulation database to provide the flow data, ray paths traced through the mean flow are compared with those traced through the actual time evolving turbulent flow. Significant scattering by the turbulence is observed. The most notable effect is that upstream traveling waves that are trapped in the potential core by the mean flow, which acts as a wave guide, easily escape in the turbulent flow. A crude statistical estimate based on ray number density suggests that directivity is modified by the turbulence, but no rigorous treatment of non-uniformities in the high-frequency approximation is attempted.

B.2 Nomenclature

a	Sound speed
N	Number of rays observed
N_r	Number or rays released
M	Mach number
p	Pressure
Re	Reynolds number
r	Radial coordinate
r_o	Jet nozzle radius
s	Entropy
t	Time
u_i	Cartesian velocities ($i = 1, 2, 3$)
x	Axial coordinate
x_i	Cartesian coordinates
α	Directivity angle
ϕ	Wave phase
ρ	Density
θ	Cylindrical polar coordinate
ω	Angular frequency

Subscripts

j	Jet exit
∞	Ambient

Accents

$\overline{()}$	Base flow (potentially time dependent)
$()'$	Acoustic perturbation

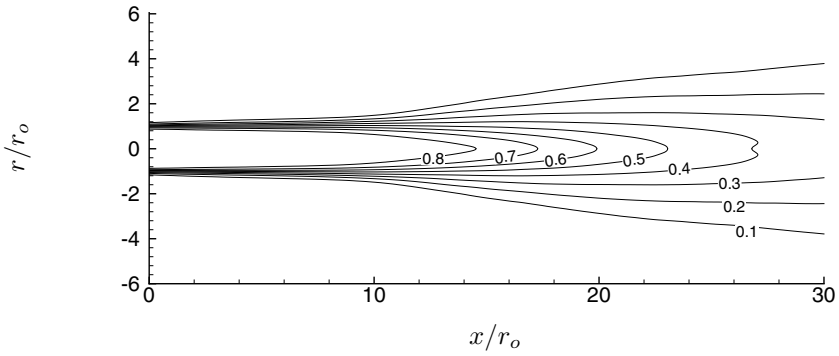

Figure 21: Contours of mean streamwise velocity: 8 evenly spaced contours from $0.1a_\infty$ to $0.8a_\infty$.

B.3 Introduction

Lighthill's theory of aerodynamic noise is often criticized because it does not distinguish refraction from generation. Instead, these effects are grouped together in a nominal 'source':[12]

$$\underbrace{\frac{\partial^2\rho}{\partial t^2} - a_\infty^2 \frac{\partial^2\rho}{\partial x_j \partial x_j}}_{\text{sound propagation}} = \underbrace{\frac{\partial^2 T_{ij}}{\partial x_i \partial x_j}}_{\text{'source'}}, \tag{19}$$

where T_{ij} is the Lighthill stress tensor. Lighthill was, of course, aware of this but concluded that refraction "may affect finer details, but it does not appear to be fundamental."[21] It has since been argued that a distinction might not be necessary when developing predictive models,[22] but since generation and propagation are different physical processes, it is attractive to model them separately. Lighthill was not faced with the stringent noise regulations that we are today. With a great effort underway to achieve as little as a 3dB noise reduction, "finer details" are now more important. More recent but more complex acoustic analogies, such Lilley's equation,[13,14]

$$\underbrace{\frac{D}{Dt}\left(\frac{D^2\Pi}{Dt^2} - \frac{\partial}{\partial x_j}\left(a^2\frac{\partial\Pi}{\partial x_j}\right)\right) + 2\frac{\partial u_k}{\partial x_j}\frac{\partial}{\partial x_k}\left(a^2\frac{\partial\Pi}{\partial x_j}\right)}_{\text{sound propagation}}$$

$$= \underbrace{-2\frac{\partial u_j}{\partial x_k}\frac{\partial u_i}{\partial x_j}\frac{\partial u_k}{\partial x_i} + (\text{viscous terms})}_{\text{source}}, \tag{20}$$

attempt to better separate propagation and generation.

Unfortunately, since (20) is nonlinear it must be linearized for implementation and interpretation.[14] An estimate of the steady mean flow is typically chosen to linearize about and many ongoing modeling endeavors take this approach.[7,24] Even modelers that circumvent the exact governing equations as a starting point and designate a relatively *ad hoc* acoustic source[36] choose to linearize about a steady mean flow. To linearize the propagation operator in (20), the nonlinear terms can be omitted, which assumes they play no substantial role at all, or moved to the right hand side, which is satisfying because the equation remains exact but once again blurs the distinction between source and propagation. Though convenient, linearization about the *mean* flow is well understood to be artificial since no individual sound wave actually encounters the mean flow.[42] Because local turbulence intensities can be over 100% in a jet, with large flow structures on the scale of the local jet radius, scattering by the turbulence might indeed be

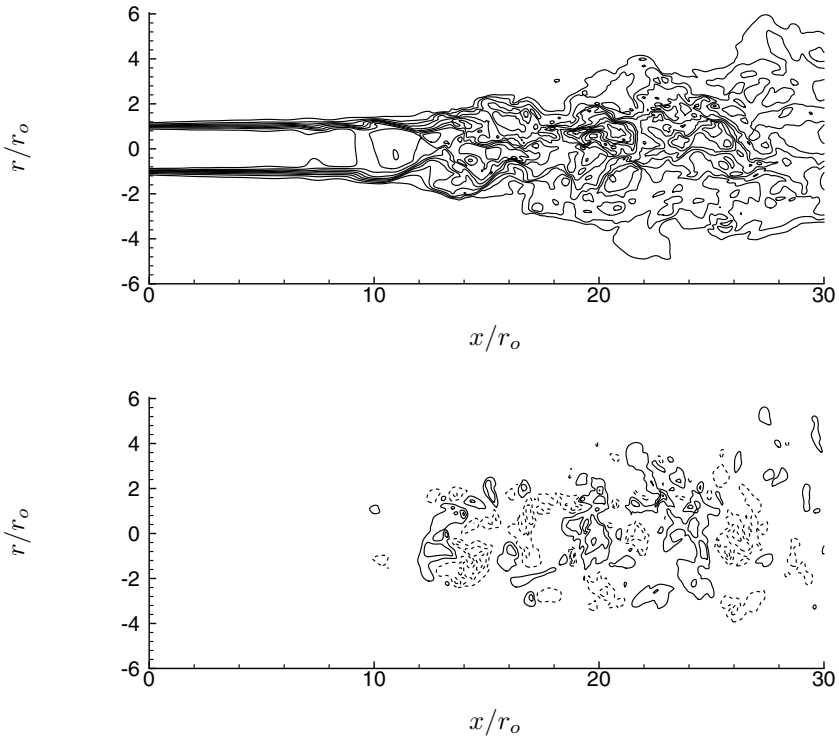

Figure 22: (a) Instantaneous axial velocity: 9 evenly spaced contours from $0.1a_\infty$ to $0.9a_\infty$. (b) Instantaneous radial velocity contours: -$0.3a_\infty$ to $0.3a_\infty$ with 0.1 spacing. Negative contours are dashed and the zero contour is omitted.

significant. We investigate this possibility.

Refraction in jets has been investigated on many fronts. In Mach 0.5 and 0.9 jets it was studied by MacGregor *et al.*[43] by adding an artificial noise source into the jets. Suzuki & Lele[44] used numerical methods and analysis to study both directional and frequency scattering of sound by instability waves in a two-dimensional mixing layer and showed a significant influence in some cases. While low frequency components of jet noise typically follow the Lighthill/Ffowcs Williams $I \propto (1 - M_c \cos\theta)^{-5}$ law, higher frequencies are less directive,[27] fit better by three inverse Doppler factors.[45] High-frequency solutions[46] of Lilley's equation for uni-directional transversely sheared flow might explain this, but scattering by turbulence has been offered as alternative explanation.[45] Similar high-frequency formulations have been incorporated into predictive tools[47,48] using a general high-frequency Green function derived by Durbin.[49] Adjoint Green functions have been proposed to simplify implementation of flow-acoustic interactions in models.[3]

The purpose of this ongoing study is to estimate the role of scattering by the unsteady turbulent fluctuations in a jet, and here we present a preliminary report on the effort. Since turbulence is analytically intractable, we rely on an existing, well-validated direct numerical simulation database to represent the turbulent jet flow. Flow-acoustic interaction is studied for high-frequency noise using an unsteady geometrical acoustic formulation to identify ray paths. Directivity is estimated statistically based on the ray paths, but no attempt has yet been made to construct instantaneous intensity profiles.

B.4 Simulation Database

Details of the direct numerical simulation database used in this study are reported in full elsewhere.[2,50,51] In summary, it is of a Reynolds number 3600, Mach number 0.9, temperature ratio $T_j/T_\infty = 0.86$ turbulent jet, which matches the experimental conditions studied by Stromberg *et al.*[1] Contours of mean streamwise velocity are shown in figure 21 and contours of instantaneous streamwise and radial velocity are shown in 22. At this Reynolds number, the initial shear layers are laminar as expected and thus qualitatively different from a high-Reynolds-number jet, which would have turbulent shear layers. However, after transition, which occurs a little before the potential core closes at $x \approx 14r_o$, the jet's development agrees well with those at a much higher Reynolds number data. Downstream of the potential core, the jet's spreading rate and Reynolds stresses agree with those of much higher Reynolds number jets.[2,52,53] This is important because it suggests that the energetic large scales are similar to those in jets at higher Reynolds numbers which should generalize the present results.

Other points of validation are reported elsewhere.[2] In these references it was shown that the mean flow, the noise directivity, and far-field noise spectrum are all in excellent agreement with the data of Stromberg *et al.*[1]

B.5 High-Frequency Approximation

High-frequency asymptotics will be used to study the interactions of sound with the flow. This approach is both convenient because it leads to tractable formulations, and important because the high frequencies are a particularly annoying component of the noise. Of course, the noise from a jet at $Re = 3600$ is relatively narrow banded compared to jets at typical engineering Reynolds numbers. However, if we accept that the large, energy carrying turbulence scales are realistic, high-frequency noise sources can be artificially added to the flow in order study flow-acoustic interactions.

It is often found that high-frequency approximations give reasonable estimates for Helmholtz numbers as low as unity,[54–56] and we will use this to estimate a lower bound on the Strouhal numbers that might be accurately represented by our procedure. We take as our length scale the 50 percent two-point velocity correlation width of the turbulent eddies, which, depending on the location within the jet, is as low as $\ell \approx 0.5r_o$.[2] This is smaller than the scale over which the mean flow varies (figure 21) except in the initial shear layers. Setting the Helmholtz number

$He \equiv \omega\ell/a = 1$ gives $\omega \approx 2a/r_o$ or $St \equiv fD/U_j = \omega 2r_o/2\pi U_j \gtrsim 1.0$. Of course, the motion of the turbulent structures might decrease or increase their effective size for a particular sound wave they encounter. Assuming $M_c \approx 0.5$, this would potentially increase the Strouhal number limit by about one-third to 1.3, which is high but still relevant for many applications.

We develop an unsteady ray tracing formulation similar to that used by Colonius *et al.*[57] We start with the Euler equations in Cartesian coordinates and three space dimensions, with the energy equation written in terms of entropy,

$$\rho\left(\frac{\partial u_i}{\partial t} + u_j\frac{\partial u_i}{\partial x_j}\right) + \frac{\partial p}{\partial x_i} = 0 \tag{21}$$

$$\frac{\partial \rho}{\partial t} + u_j\frac{\partial \rho}{\partial x_j} + \rho\frac{\partial u_j}{\partial x_j} = 0 \tag{22}$$

$$\frac{\partial s}{\partial t} + u_j\frac{\partial s}{\partial x_j} = 0, \tag{23}$$

and decompose the dependent variables as

$$\begin{bmatrix}\rho\\ u_i\\ p\\ s\end{bmatrix}_{(x_i,t)} = \begin{bmatrix}\bar{\rho}\\ \bar{u}_i\\ \bar{p}\\ \bar{s}\end{bmatrix}_{(x_i,t)} + \begin{bmatrix}\rho'\\ u_i'\\ p'\\ s'\end{bmatrix}_{(x_i,t)}, \tag{24}$$

where $\overline{()}$ terms will be obtained from the simulation database and in general are functions of all space coordinates and time. The $()'$ terms are perturbations, but not necessarily acoustic at this point. Retaining only linear terms in the perturbations gives

$$\frac{\partial u_i'}{\partial t} + \bar{u}_j\frac{\partial u_i'}{\partial x_j} + u_j'\frac{\partial \bar{u}_i}{\partial x_j} + \frac{\rho'}{\bar{\rho}}\left(\frac{\partial \bar{u}_i}{\partial t} + \bar{u}_j\frac{\partial \bar{u}_i}{\partial x_j}\right) + \frac{1}{\bar{\rho}}\frac{\partial p'}{\partial x_i} = 0 \tag{25}$$

$$\frac{\partial \rho'}{\partial t} + \bar{u}_j\frac{\partial \rho'}{\partial x_j} + \bar{\rho}\frac{\partial u_j'}{\partial x_j} + \rho'\frac{\partial \bar{u}_j}{\partial x_j} + u_j'\frac{\partial \bar{\rho}}{\partial x_j} = 0 \tag{26}$$

$$\frac{\partial s'}{\partial t} + \bar{u}_j\frac{\partial s'}{\partial x_j} + u_j'\frac{\partial \bar{s}}{\partial x_j} = 0. \tag{27}$$

We next assume harmonic fluctuations

$$\begin{bmatrix}u_i'\\ \rho'\\ p'\\ s'\end{bmatrix} = \begin{bmatrix}U_i\\ R\\ P\\ S\end{bmatrix} e^{i\omega\phi(x_i,t)}, \tag{28}$$

where U_i, R, P and S are complex amplitudes that are functions of (x_i, t), ϕ is a real-valued phase function, and ω is the (large) angular frequency of the disturbances. Substituting and retaining only the highest order terms in ω yields

$$\left(\frac{\partial \phi}{\partial t} + \bar{u}_j\frac{\partial \phi}{\partial x_j}\right)U_i + \frac{\bar{p}}{\bar{\rho}}\frac{\partial \phi}{\partial x_i}S + \frac{\bar{a}^2}{\bar{\rho}}\frac{\partial \phi}{\partial x_i}R = 0 \tag{29}$$

$$\left(\frac{\partial \phi}{\partial t} + \bar{u}_j\frac{\partial \phi}{\partial x_j}\right)R + \bar{\rho}\frac{\partial \phi}{\partial x_j}U_j = 0 \tag{30}$$

$$\left(\frac{\partial \phi}{\partial t} + \bar{u}_j\frac{\partial \phi}{\partial x_j}\right)S = 0. \tag{31}$$

This leaves 5 equations and 5 unknowns. For a non-trivial solution the determinant of this

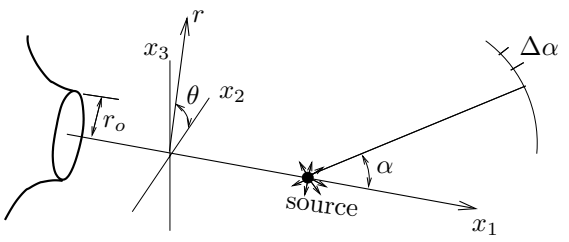

Figure 23: Coordinate system schematic.

system must be zero:

$$G^3\left[G^2 - \bar{a}^2\left(\frac{\partial\phi}{\partial x_j}\frac{\partial\phi}{\partial x_j}\right)\right] = 0, \tag{32}$$

where $G = \frac{\partial\phi}{\partial t} + \bar{u}_j\frac{\partial\phi}{\partial x_j}$. It is obvious that $G^3 = 0$ roots correspond to vorticity and entropy modes and are therefore not of concern to us. The remaining equation can be solved by method of characteristics to yield a system of ordinary differential equations for the ray paths,

$$\frac{dx_i}{dt} = \bar{u}_i - \frac{\bar{a}^2\phi_{x_i}}{\phi_t + \bar{u}_j\phi_{x_j}} \tag{33}$$

$$\frac{d\phi_{x_i}}{dt} = -\frac{\partial\bar{u}_j}{\partial x_i}\phi_{x_j} + \frac{\partial\bar{a}^2}{\partial x_i}\frac{\phi_{x_j}\phi_{x_j}}{\phi_t + \bar{u}_j\phi_{x_j}} \tag{34}$$

$$\frac{d\phi_t}{dt} = -\frac{\partial\bar{u}_j}{\partial t}\phi_{x_j} + \frac{\partial\bar{a}^2}{\partial t}\frac{\phi_{x_j}\phi_{x_j}}{\phi_t + \bar{u}_j\phi_{x_j}} \tag{35}$$

$$\frac{d\phi}{dt} = 0, \tag{36}$$

where subscripts on ϕ indicate partial differentiation.

Once an initial coordinate is chosen, initial conditions for ϕ_{x_i} are determined by solving (33) with $\phi_t = r_o/a_\infty$ and

$$\frac{d}{dt}\begin{bmatrix}x_1\\x_2\\x_3\end{bmatrix} = \begin{bmatrix}\bar{a}\cos\alpha + \bar{u}_1\\ \bar{a}\sin\alpha\,\cos\theta + \bar{u}_2\\ \bar{a}\sin\alpha\,\sin\theta + \bar{u}_3\end{bmatrix}. \tag{37}$$

The results are insensitive to the choice of ϕ_t and, as we shall see, (35) in general.

B.6 Procedure

Equations (33) through (36) were integrated using a fourth-order Runge–Kutta algorithm with $\Delta t = 0.01 r_o/a_\infty$. Coefficients $\bar{u}_i$ and $\bar{a}$ were taken from the direct numerical simulation database. This data was available every $\Delta t = 0.17 r_o/a_\infty$ and at every other mesh point of the original computation. It was interpolated in space using B-splines and in time using a linear method. Differences were computed using second-order centered finite differences with $\delta = 0.001 r_o$. Results were insensitive to this value and did not change if a fourth-order finite difference was used instead. Results were also insensitive to the order of the B-spline used. We traced $N_r = 1000$ rays through the mean-flow and $N_r = 500$ rays through the unsteady flow. They were initially directed at evenly spaced α-angles in the $\theta = 0, \pi$ and $\theta = \pm\pi/2$ planes (see figure 23). Results shown here were insensitive to the number of rays traced. Except when noted, rays were traced for a total time of $25.5 r_o/a_\infty$.

Focusing by the turbulence will cause ray path to cross at points in their trajectories. At these caustics, the high-frequency approximation for amplitude, which can be obtained from the next highest terms in ω, fails because the wave fronts develop cusps, a feature that is always small

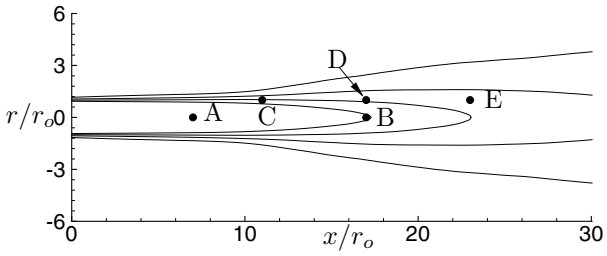

Figure 24: Schematic showing source points used. See also table 4.

Case	x/r_o	r/r_o
A	7	0
B	17	0
C	11	1
D	17	1
E	23	1

Table 4: Source points (see figure 24). All have $\theta = 0$.

with respect to a wavelength of the sound. In addition, behind the caustics multiple rays pass through each point and potentially interfere with each other. Even in a steady case with simply defined caustics, a rigorous solution in regions of multiple rays adds considerable complexity. In the present case where caustics are numerous, transitory and impossible to anticipate, we have not undertaken the task of developing a uniformly valid amplitude procedure. Instead, to estimate the effect of refraction on directivity we simply count the number of rays passing through different regions on a sphere surrounding the source. The resulting ray number density, N, can be shown inversely related to ray tube area, A, and thus proportional to tube intensity, I, which is valid where there are no caustics. We assume that the volume of the caustic-affected region crossing the observation sphere is negligible and the positions of the caustics ever changing, as is indeed observed, and can therefore neglect them in the statistical average. We also assume that behind the caustics the rays are decorrelated due to the stochastic action of the turbulence so we also neglect interference. The results of these assumptions is a statistical beam-like method which provides an estimate of directivity.

Ray position statistics were accumulated as they exited a sphere of radius $r = 6.0r_o$ centered on the jet axis closest to the source. Monitoring a sphere at $r = 10r_o$ instead of $r = 6.0r_o$ caused a negligible change in our results. These data were collected in 20 bins of width $\Delta\alpha$ (see figure 23). Some rays were trapped in the jet, usually in the initial shear layers that act as a wave guide, and did not reach this spherical surface in the run time. These rays were not counted on the assumption they would have dissipated or entered the nozzle. Using a run time of $10r_o/a_\infty$ did not change the directivity estimates for $\alpha \lesssim 150°$. For the unsteady case, rays were traced through 39 separate time series that were separated in initial times by at least one large-eddy turnover time. The turbulence evolved as the rays progressed.

B.7 Results and Conclusions

The five point-source positions studied are labeled in figure 24 and summarized in table 4. The ray number-density directivities for all cases are plotted in figure 25 (a-e). In figure 25 (a), where the source is in the laminar potential core region ($x = 7r_o, r = 0$), we see little difference

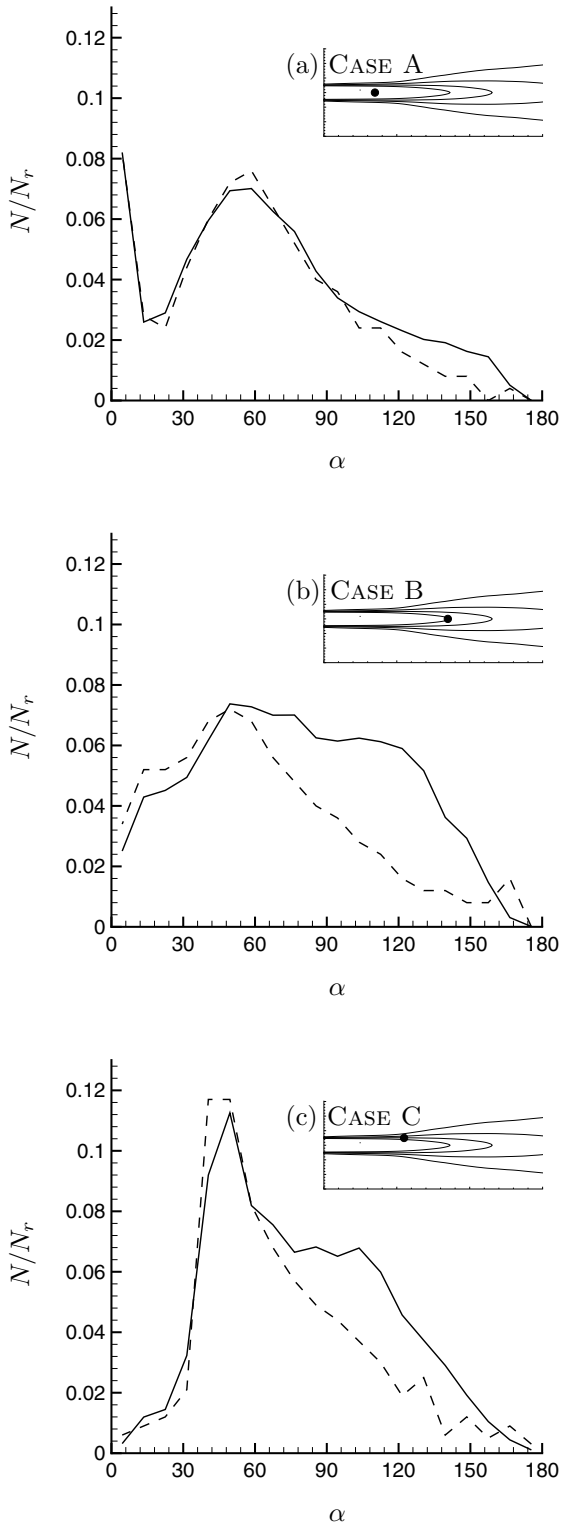

Figure 25: Figure continues on the following page.

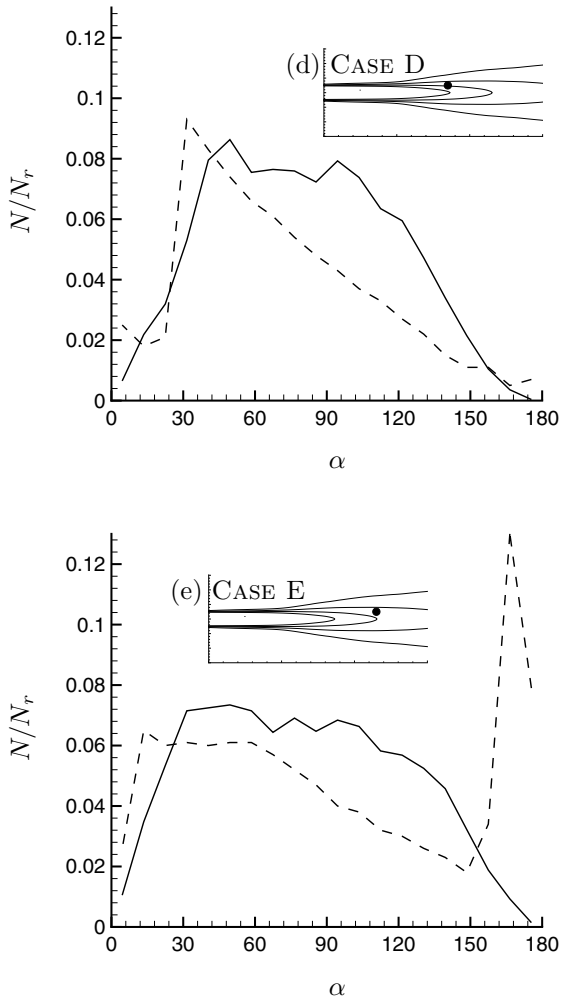

Figure 25: (a-e) Bin number density for rays traced through mean ---- and turbulent —— jet flows. See table 4 for source points.

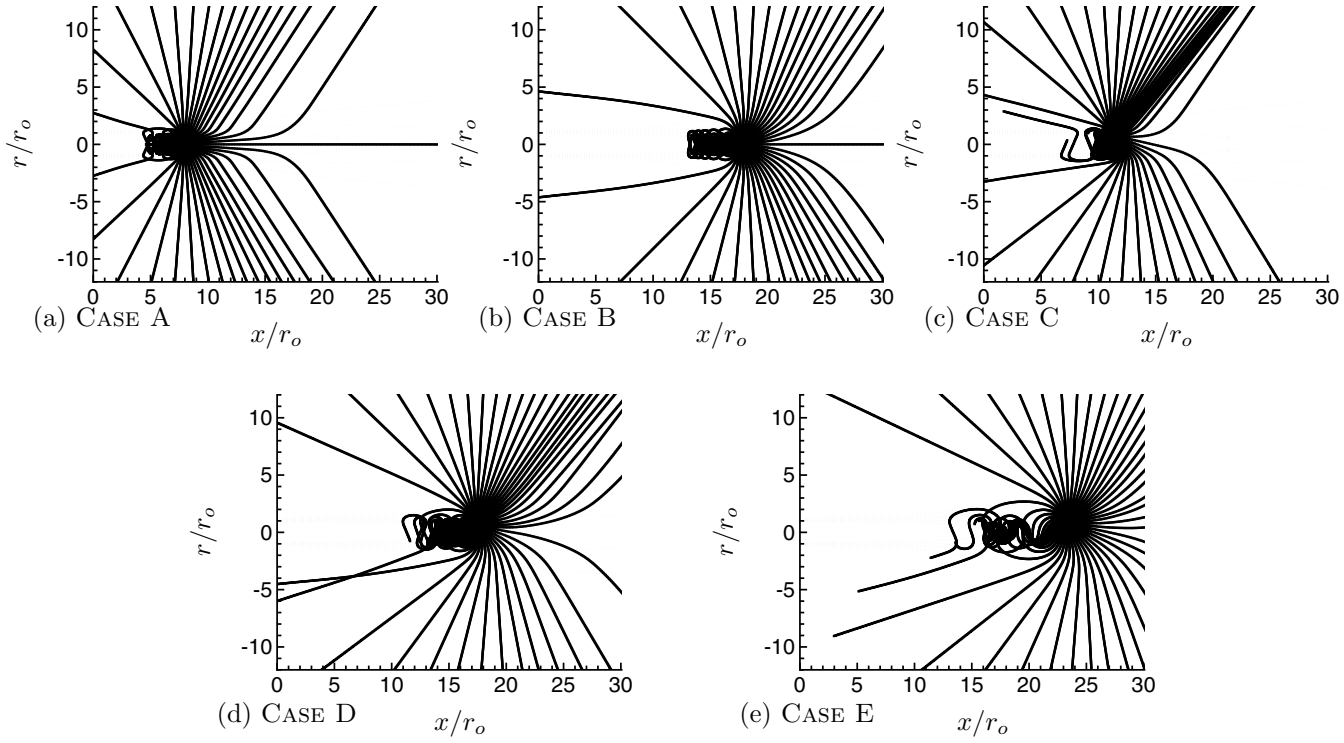

Figure 26: Every tenth ray path released in the x–y plane in the mean flow for labeled cases (see table 4).

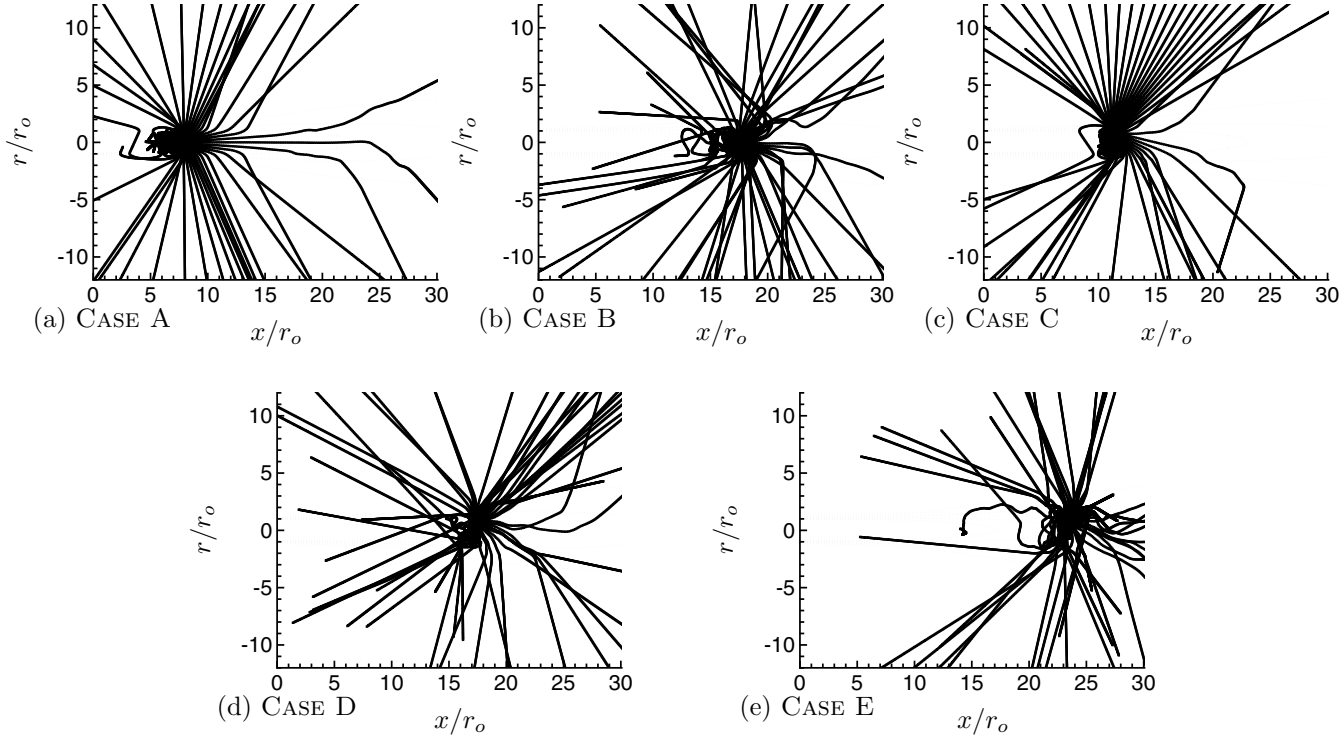

Figure 27: Every fifth ray released in the x–y plane in the unsteady flow for the labeled cases (see table 4).

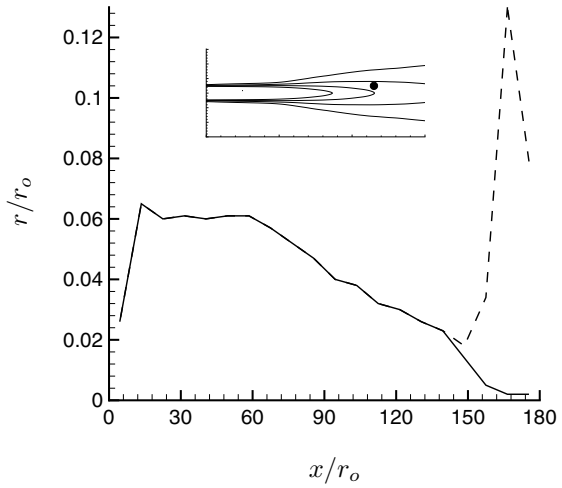

Figure 28: Mean flow ray number-density directivity for trace times of $10r_o/a_\infty$ —— and $25r_o/a_\infty$ ---- . CASE E is shown.

between the steady and unsteady ray number-density directivity. However, for rays released on the jet's axis just past the end of the potential core at $x = 17r_o$ (figure 25 b), there is a significant difference between the two cases. In the mean-flow case, substantially fewer rays leave the observation sphere at angles greater than $\alpha = 70°$. The reason for this is clear in figure 26 (b): the upstream traveling waves are trapped by the jet's shear layers. However, in the unsteady case the rays escape and radiate as seen in figure 27 (b). Other source points are seen to give similar results.

The freeing of trapped rays appears to be the principle difference between the steady and unsteady cases for all the source points considered. In figure 25 (e), the upstream velocity is slow enough that trapped upstream traveling waves appear as a spike in the profile near $\alpha = 180°$ at the observation time. The trapped rays must eventually escape or enter the nozzle. Whether they will eventually affect the directivity is unclear, but the rate of release is slow: the steady-flow number-density directivity is unchanged for ray trace times of $10r_o/a_\infty$ versus $25r_o/a_\infty$ for $\alpha \lesssim 150°$ (see figure 28). If they do eventually leave the jet, they will do so differently than the rays in a realistic turbulent jet.

So far we have assumed that the source itself has no inherent directivity. However, if the sources are convecting quadrupoles, this is not true. In figures 29 (a-e) the rays have been given an initial weighting so that they would have a three Doppler factor, $W^{-3} = (1 - M_c \cos\alpha)^{-3}$, directivity in absence of additional refraction. The convection Mach number was taken to be $M_c = 0.5$, which corresponds to a convection velocity of $U_c = 0.6U_j$. We again see significant influence of the turbulence on the directivity estimates.

It is interesting to estimate how much of the scattering is because of the presences of the turbulence at any instance in time versus its change in time. To this end we have plotted a directivity for case B with the time derivative terms of the background flow in (36) set to zero. We compare with the correct equation results in figure 30, and see that there is an effect for $\alpha \gtrsim 60°$, but not a large one. It appears that accounting for the turbulence as a succession of steady states would provide most of the scattering.

In summary, we have made a crude estimate of the effect of turbulence on the propagation of high-frequency noise in turbulent jets and found that turbulence does affect the ray number density on a spherical surface outside the jet, increasing it in most cases. The most significant mechanism observed was that the turbulence frees rays that would otherwise be trapped traveling upstream in the potential core if only refraction by the mean flow were considered. The spatial

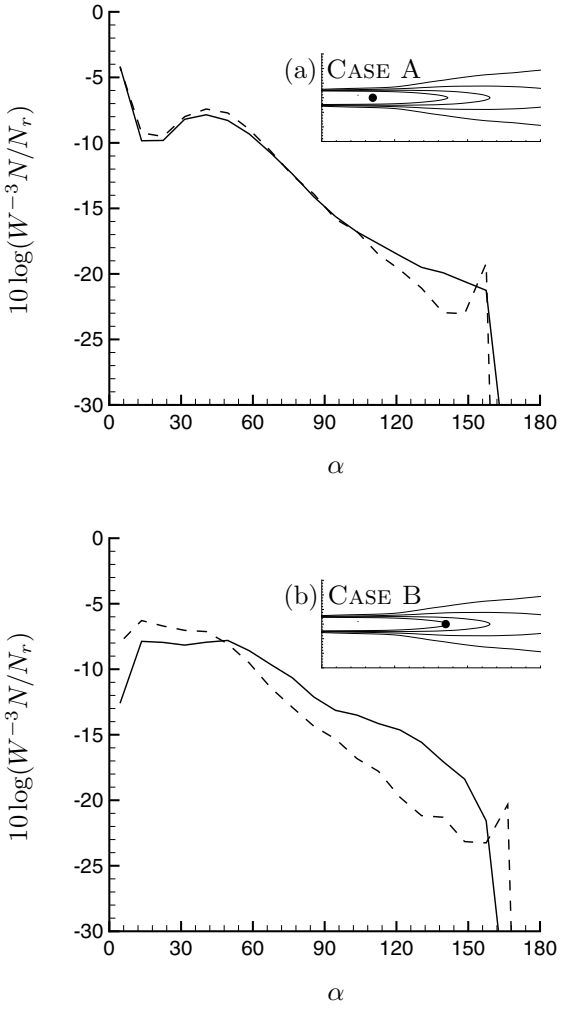

Figure 29: Figure continues on page 33.

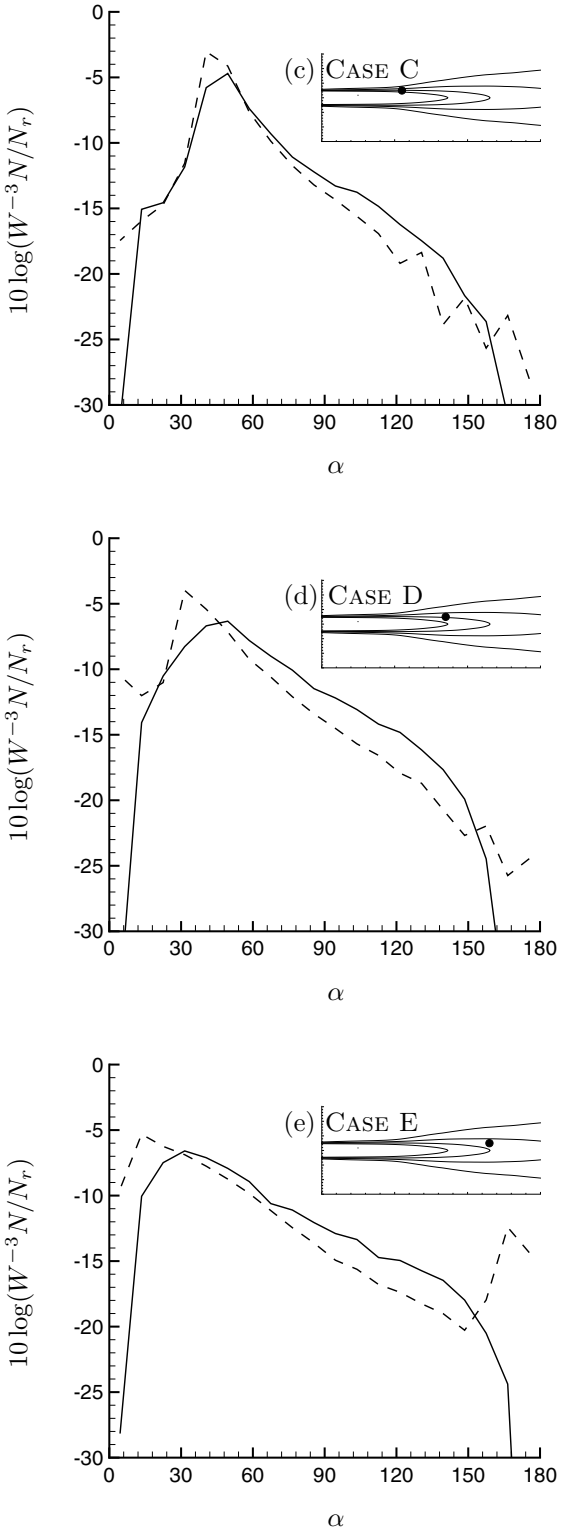

Figure 29: (a-e) Directivity when rays are given an effective three Doppler factors weighting.

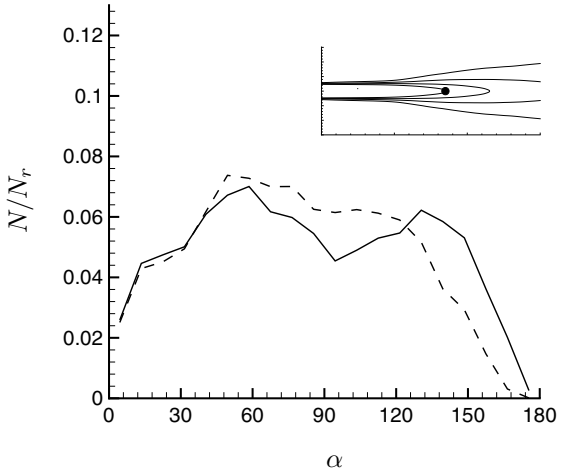

Figure 30: Directivity for CASE B, $x = 17r_o, r = 0$, with time derivatives in (35) ---- and without ——— .

variation of the turbulence was found to be more an influence on scattering than its time evolution.

This work is ongoing and a rigorous means of computing directivity as well as more realistic sources are being considered.

B.8 Acknowledgments

Support for this work provided by NASA is very gratefully acknowledged.

References

[1] J. L. Stromberg, D. K. McLaughlin and T. R. Troutt, "Flow field and acoustic properties of a Mach number 0.9 jet at a low Reynolds number," J. of Sound and Vib. **72**, 159 (1980).

[2] J. B. Freund, "Noise sources in a low-Reynolds-number turbulent jet at Mach 0.9," J. Fluid Mech. **438**, 277 (2001).

[3] C. K. W. Tam and L. Auriault, "Mean flow refraction effects on sound radiated from localized sources in a jet," J. Fluid Mech. **370**, 149 (1998).

[4] J. B. Freund, S. K. Lele and P. Moin, "Direct numerical simulation of a Mach 1.92 turbulent jet and its sound field," AIAA J. **38**, 2023 (2000).

[5] K. Mohseni, T. Colonius and J. B. Freund, "An evaluation of linear instability waves as sources of sound in a supersonic turbulent jet," Phys. Fluids **14**, tba (2002).

[6] H. S. Ribner, "Quadrupole correlations governing the pattern of jet noise," J. Fluid Mech. **38**, 1 (1969).

[7] A. Khavaran, "Role of anisotropy in turbulent mixing noise," AIAA J. **37**, 832 (1999).

[8] A. Khavaran, "Influence of mean-density gradient on small-scale turbulence noise," Sixth AIAA/CEAS Aeroacoustics Conference, Lahaina, Hawaii, AIAA Paper 2000-2059 (2000).

[9] A. Khavaran, J. Bridges and J. B. Freund, "A parametric study of fine-scale turbulence mixing noise," AIAA Paper 2002-2419 (2002).

[10] C. Bailly, P. Lafon and S. Candel, "Subsonic and supersonic jet noise predictions from statistical source models," AIAA J. **35**, 1688 (1997).

[11] T. F. Balsa, "The acoustic field of sources in shear flow with application to jet noise: convective amplification," J. Fluid Mech. **79**, 33 (1977).

[12] M. J. Lighthill, "On sound generated aerodynamically: I. General theory," Proc. Royal Soc. Lond. A **211**, 564 (1952).

[13] G. M. Lilley, "On the noise from jets," Technical Report CP-131, AGARD (1974).

[14] M. E. Goldstein, *Aeroacoustics* (McGraw-Hill Book Co.) (1976).

[15] G. M. Lilley, "Jet noise: Classical theory and experiments," In *Aeroacoustics of Flight Vehicles* edited by H. Hubbard. NASA RP 1258 (1991).

[16] D. G. Crighton, "Basic principles of aerodynamic noise generation," Progress in Aerospace Sciences **16**, 31 (1975).

[17] G. M. Lilley, "Othe radiated noise from isotripic turbulence with applications to the theory of jet noise," J. of Sound and Vib. **190**, 463 (1996).

[18] T. Colonius and J. B. Freund, "Application of Lighthill's equation to a Mach 1.92 turbulent jet," AIAA J. **38**, 368 (2000).

[19] M. J. Lighthill, "An estimate of the covariance of t_{xx} without using statistical assumptions," Appendix 1 of "On the noise radiated from a turbulent high speed jet", by G. M. Lilley in *Computational Aeroacoustics* edited by J. C. Hardin and M. K. Hussaini, New York: Springer-Verlag. (1992).

[20] S. Narayanan, T. Barber and D. Polak, "High subsonic jet experiments. Part II: Turbulence and noise generation studies," AIAA/CEAS Aeroacoustics Conference and Exhibit, 6th, Maui, AIAA Paper 2000-2023 (2000).

[21] M. J. Lighthill, "On sound generated aerodynamically: II. Turbulence as a source of sound," Proc. Royal Soc. Lond. A **222**, 1 (1954).

[22] C. Bailly, P. Lafon and S. Candel, "Computation of subsonic and supersonic jet mixing noise using a modified k–ε model for compressible free shear flows," Acta Acustica **2**, 101 (1994).

[23] W. Béchara, P. Lafon, C. Bailly and S. Candel, "Application of the k-ε turbulence model to the prediction of noise from simple and coaxial free jets," J. of Acoust. Soc. Am. **97**, 3518 (1995).

[24] A. Khavaran, E. A. Krejsa and C. M. Kim, "Computation of supersonic jet mixing noise for an axisymmetric convergent-divergent nozzle," J. Aircraft **31**, 603 (1994).

[25] B. E. Mitchell, S. K. Lele and P. Moin, "Direct computation of the sound generated by subsonic and supersonic axisymmetric jets," Technical Report TF-66, Stanford University, Mechanical Engineering (November 1995).

[26] G. M. Lilley, "Jet noise: Classical theory and experiments," in H. Hubbard, editor, *Aeroacoustics of Flight Vehicles*, volume 1, pages 211–289 (Acous. Soc. Am., New York) (1995).

[27] P. A. Lush, "Measurements of subsonic jet noise and comparison with theory," J. Fluid Mech. **46**, 477 (1971).

[28] M. E. Goldstein, "The low frequency sound from multipole sources in axisymmetric shear flows, with applications to jet noise," J. Fluid Mech. **70**, 595 (1975).

[29] M. E. Goldstein and B. M. Rosenbaum, "Effect of anisotripic turbulence on aerodynamic noise," J. of Acoust. Soc. Am. **54**, 630 (1973).

[30] H. K. Tanna, M. J. Fisher and P. D. Dean, "Effects of temperature on supersonic jet noise," AIAA Paper 73-991 (1973).

[31] J. E. Ffowcs Williams, "The noise from turbulence convected at high speed," Phil. Trans. Roy. Soc. A **255**, 469 (1963).

[32] J. B. Freund and T. G. Fleischman, "Ray traces through unsteady jet turbulence," Int. J. Aeroacoustics **1**, 83 (2002).

[33] B. E. Mitchell, S. K. Lele and P. Moin, "Direct computation of the sound generated by vortex pairing in an axisymmetric jet," J. Fluid Mech. **383**, 113 (1999).

[34] M. J. Lighthill, "Jet noise," AIAA J. **1**, 1507 (1963).

[35] C. K. W. Tam, "Jet noise: since 1952," Theoret. Comp. Fluid Dyn. **10**, 393 (1998).

[36] C. K. W. Tam and L. Auriault, "Jet mixing noise from fine-scale turbulence," AIAA J. **37**, 145 (1999).

[37] G. K. Batchelor, *The theory of homogenous turbulence* (Cambridge University Press, Cambridge) (1960).

[38] J. Bridges and M. P. Wernet, "Turbulence measurents of separated flow nozzles with mixing enhancement features," AIAA Paper 2002-2484 (2002).

[39] G. M. Lilley, "The radiated noise from isotropic turbulence revisited," ICASE Report 93-75 (December 1993).

[40] H. K. Tanna, "An experimental study of jet noise. Part I. Turbulent mixing noise," J. of Sound and Vib. **50**, 405 (1977).

[41] J. B. Freund and S. K. Lele, "Computer simulation and prediction of jet noise," (2001).

[42] A. P. Dowling, J. P. Ffowcs Williams and M. E. Goldstein, "Sound propagation in a moving stream," Phil. Trans. Roy. Soc. Lond. A **288**, 321 (March 1978).

[43] G. R. MacGregor, H. S. Ribner and H. Lam, "'basic' jet noise patterns after delection of convection and refractioneffects: experiments vs. theory," J. of Sound and Vib. **27**, 437 (1973).

[44] T. Suzuki and S. K. Lele, "Acoustic scattering from a mixing layer: role of instability waves," AIAA Paper 99-0228 (1999).

[45] M. E. Goldstein, "Aeroacoustics of turbulent shear flows," Ann. Rev. Fluid Mech. **16** (1984).

[46] M. E. Goldstein, "High frequency sound emission from moving point multipole sources embedded in arbitrary transversely sheared mean flows," J. of Sound and Vib. **80**, 499 (1982).

[47] A. Khavaran and E. A. Krejsa, "Propagation of high frequency jet noise using geometric acoustics," 31st Aerospace Sciences Meeting, Reno, NV, AIAA Paper 93-0147 (January 1993).

[48] A. Khavaran and E. A. Krejsa, "Refraction of high frequency jet noise in an arbitrary jet flow," 32nd Aerospace Sciences Meeting, Reno, NV, AIAA Paper 93-0147 (January 1994).

[49] P. A. Durbin, "High frequency Green function for aerodynamic noise in moving media, Part 1: General theory," J. of Sound and Vib. **91**, 519 (1983).

[50] J. B. Freund, "Direct numerical simulation of the noise from a Mach 0.9 jet," ASME FEDSM99-7251 (1999).

[51] J. B. Freund, "Acoustic sources in a turbulent jet: a direct numerical simulation study," AIAA Paper 99-1858 (1999).

[52] H. J. Hussein, S. P. Capp and W. K. George, "Velocity measurements in a high-Reynolds-number, momentum-conserving, axisymmetric, turbulent jet," J. Fluid Mech. **258**, 31 (1994).

[53] N. R. Panchapakesan and J. L. Lumley, "Turbulence measurements in axisymmetric jets of air and helium. Part 1. Air jets," J. Fluid Mech. **246**, 197 (1993).

[54] T. F. Balsa, "The far field of high frequency convected singularities in sheared flows, with application to jet noise prediction," J. Fluid Mech. **74**, 193 (1976).

[55] B. J. Tester and C. L. Morfey, "Developments in jet noise modeling – theoretical predicitons and comparisons with measured data," J. of Sound and Vib. **46**, 79 (1976).

[56] J. N. Scott, "Propagation of sound waves through linear shear layers," AIAA J. **17**, 237 (1979).

[57] T. Colonius, S. K. Lele and P. Moin, "The scattering of sound waves by a compressible vortex–numerical simulations and analytical solutions," J. Fluid Mech. **260**, 271 (1994).

REPORT DOCUMENTATION PAGE

Form Approved
OMB No. 0704-0188

1. AGENCY USE ONLY (*Leave blank*)	2. REPORT DATE	3. REPORT TYPE AND DATES COVERED
	February 2003	Interim Contractor Report

4. TITLE AND SUBTITLE

Jet Noise Physics and Modeling Using First-Principles Simulations

5. FUNDING NUMBERS

WBS–22–708–87–23
NAG3–2662

6. AUTHOR(S)

Jonathan B. Freund

7. PERFORMING ORGANIZATION NAME(S) AND ADDRESS(ES)

University of Illinois, Urbana-Champaign
Department of Theoretical and Applied Mechanics
Urbana, Illinois 62801

8. PERFORMING ORGANIZATION REPORT NUMBER

E–13775

9. SPONSORING/MONITORING AGENCY NAME(S) AND ADDRESS(ES)

National Aeronautics and Space Administration
Washington, DC 20546–0001

10. SPONSORING/MONITORING AGENCY REPORT NUMBER

NASA CR—2003-212123

11. SUPPLEMENTARY NOTES

Project Manager, James E. Bridges, Structures and Acoustics Division, NASA Glenn Research Center, organization code 5940, 216–433–2963.

12a. DISTRIBUTION/AVAILABILITY STATEMENT

Unclassified - Unlimited
Subject Categories: 07 and 34 Distribution: Nonstandard

Available electronically at http://gltrs.grc.nasa.gov

This publication is available from the NASA Center for AeroSpace Information, 301–621–0390.

12b. DISTRIBUTION CODE

13. ABSTRACT ***(Maximum 200 words)***

An extensive analysis of our jet DNS database has provided for the first time the complex correlations that are the core of many statistical jet noise models, including MGBK. We have also for the first time explicitly computed the noise from different components of a commonly used noise source as proposed in many modeling approaches. Key findings are: (1) While two-point (space and time) velocity statistics are well-fitted by decaying exponentials, even for our low-Reynolds-number jet, spatially integrated fourth-order space/retarded-time correlations, which constitute the noise "source" in MGBK, are instead well-fitted by Gaussians. The width of these Gaussians depends (by a factor of 2) on which components are considered. This is counter to current modeling practice, (2) A standard decomposition of the Lighthill source is shown by direct evaluation to be somewhat artificial since the noise from these nominally separate components is in fact highly correlated. We anticipate that the same will be the case for the Lilley source, and (3) The far-field sound is computed in a way that explicitly includes all quadrupole cancellations, yet evaluating the Lighthill integral for only a small part of the jet yields a far-field noise far louder than that from the whole jet due to missing non-quadrupole cancellations. Details of this study are discussed in a draft of a paper included as appendix A.

14. SUBJECT TERMS

Jet noise; CFD; Jet; Acoustic; Noise prediction

15. NUMBER OF PAGES

48

16. PRICE CODE

17. SECURITY CLASSIFICATION OF REPORT	18. SECURITY CLASSIFICATION OF THIS PAGE	19. SECURITY CLASSIFICATION OF ABSTRACT	20. LIMITATION OF ABSTRACT
Unclassified	Unclassified	Unclassified	